

Transmission of Rossby waves through the Philippine Archipelago

Mac Euan Ducusin Malugao¹, Sen Jan², Ming-Huei Chang², Tung-Yuan Ho³, and Yiing Jang Yang²

¹Mindanao State University - Iligan Institute of Technology

²National Taiwan University

³Academia Sinica

December 27, 2023

Abstract

Oceanic Rossby waves play a crucial role in shaping the physical and biological dynamics of both open and coastal oceans, especially within the tropical band spanning between the 10°S and 10°N parallels. Yet, the extent to which Rossby waves can transmit and impact the hydrography and ecosystem of semi-enclosed seas like the South China Sea (SCS) remains unclear. This study aims to investigate the transmission of Rossby waves through the Philippine archipelago, using satellite altimeter-derived sea level anomaly (SLA) and coastal tide gauge records. Our findings reveal that westward-propagating Rossby waves in the tropical Pacific Ocean with a wave speed of ~ 0.64 m s⁻¹ first entered the Celebes Sea, and then passed through the Sibutu Passage into the Sulu Sea from April to December 2017. Subsequently, the waves propagated along the northeast coast of Sabah and the east coast of Palawan before exiting through the Mindoro Strait to the central SCS. Additionally, a β -refracted Rossby wave with wave speed of 0.28 m s⁻¹ also penetrated the archipelago but at a latitude further north $\sim 10^\circ$ N from July to November via Surigao Strait and propagated toward the south and north of Palawan, ultimately reaching the west coast of Palawan in the eastern central SCS. This study verifies that the transmission of Rossby waves originating from the east of the Philippines could induce intraseasonal sea level oscillations off Palawan, which could subsequently propagate westward across the central SCS as identified in previous field observations.

Hosted file

982296_0_supp_11699251_s5q71q.docx available at <https://authorea.com/users/711043/articles/695462-transmission-of-rossby-waves-through-the-philippine-archipelago>

Transmission of Rossby waves through the Philippine Archipelago

Mac Euan D. Malugao^{1,2,5}, Sen Jan³, Ming-Huei Chang³, Tung-Yuan Ho^{1,3,4}, Yiing Jang Yang³

¹ Earth System Science Program, Taiwan International Graduate Program, Academia Sinica, Taipei, Taiwan, R.O.C.

² Taiwan International Graduate Program for Earth System Science, National Taiwan University, Taipei, Taiwan, R.O.C.

³ Institute of Oceanography, National Taiwan University, Taipei, Taiwan, R.O.C.

⁴ Research Center for Environmental Changes, Academia Sinica, Taipei, Taiwan, R.O.C.

⁵ Department of Marine Science, College of Science and Mathematics, Mindanao State University – Iligan Institute of Technology, Iligan City, Philippines

Corresponding author: Sen Jan (senjan@ntu.edu.tw)

Key Points:

- Satellite altimeter proved Rossby wave transmission through the Philippine archipelago and into central South China Sea.
- Rossby waves entered Celebes Sea and passed Sibutu Passage into Sulu Sea, while β -refracted Rossby wave entered Sulu Sea via Surigao Strait.
- The Mindoro Strait and the Balabac Strait served as gateways for the Rossby waves entering the central South China Sea from the Sulu Sea.

Abstract

Oceanic Rossby waves play a crucial role in shaping the physical and biological dynamics of both open and coastal oceans, especially within the tropical band spanning between the 10°S and 10°N parallels. Yet, the extent to which Rossby waves can transmit and impact the hydrography and ecosystem of semi-enclosed seas like the South China Sea (SCS) remains unclear. This study aims to investigate the transmission of Rossby waves through the Philippine archipelago, using satellite altimeter-derived sea level anomaly (SLA) and coastal tide gauge records. Our findings reveal that westward-propagating Rossby waves in the tropical Pacific Ocean with a wave speed of $\sim 0.64 \text{ m s}^{-1}$ first entered the Celebes Sea, and then passed through the Sibutu Passage into the Sulu Sea from April to December 2017. Subsequently, the waves propagated along the northeast coast of Sabah and the east coast of Palawan before exiting through the Mindoro Strait to the central SCS. Additionally, a β -refracted Rossby wave with wave speed of 0.28 m s^{-1} also penetrated the archipelago but at a latitude further north $\sim 10^\circ\text{N}$ from July to November via Surigao Strait and propagated toward the south and north of Palawan, ultimately reaching the west coast of Palawan in the eastern central SCS. This study verifies that the transmission of Rossby waves originating from the east of the Philippines could induce intraseasonal sea level oscillations off Palawan, which could subsequently propagate westward across the central SCS as identified in previous field observations.

40

Keywords: Sea level anomaly, satellite altimeter, Hovmöller diagram, first baroclinic mode, western boundary

Plain Language Summary

Oceanic Rossby waves are like movers shaping how things work in the world's oceans, especially in tropical bands between 10 degrees south and 10 degrees north of the equator. We wanted to figure out how these waves travel and affect seas like the South China Sea. Using data from satellites and measurements along the coast, we discovered that these waves, traveling at about 0.64 meters per second, first went through the Celebes Sea, then moved through specific passages to reach the Sulu Sea between April and December 2017. Another type of Rossby wave traveled at a different speed through a different route, arriving at the same destination in the South China Sea. This research helps us understand how these waves move through the Philippine islands and impact sea levels around them.

53 **1. Introduction**

54 Large-scale westward-propagating oceanic Rossby waves, which can be identified from
55 sea level anomalies observed by satellites, significantly impact the sea surface height variations,
56 geostrophic current, and hydrography in the ocean and the weather and climate from the
57 atmospheric variations during their journey across the entire basin (Chelton & Schlax, 1996;
58 Jacobs et al., 1993). They transport heat in the meridional direction, regulate the climate,
59 redistribute the water mass and nutrients in the ocean, and shape the ocean circulation (e.g.,
60 Anderson & Gill, 1975; Jacobs et al., 1994; Meyers et al., 1996; Stammer et al., 2008; Uz et al.,
61 2001; White et al., 1998). The formation of Rossby waves may originate from wind burst forcing
62 (Anderson et al., 1979; Cabanes et al., 2006; Qiu, 2003), the reflection of Kelvin waves in the
63 eastern boundary (Delcroix et al., 1991; Jacobs et al., 1994; McCreary, 1976), or buoyancy
64 forcing (Piecuch & Ponte, 2012). As Rossby waves approach the western boundary, they can
65 intensify the western boundary current (Anderson et al., 1979; Anderson & Gill, 1975), modulate
66 local sea-level annual cycles (Calafat et al., 2018), and reflect from the western boundary to form
67 Kelvin waves propagating eastward along the equator (du Penhoat & Cane, 1991; White, 2000;
68 Zang et al., 2002). In addition to their importance in ocean dynamics, du Penhoat and Cane
69 (1991) and Spall and Pedlosky (2005) suggested that, as a first mode baroclinic Rossby wave
70 impinges on a small meridional gap in the western boundary, a considerable portion of incident
71 wave energy can transmit through the gap, while wave energy and, in turn, amplitude of reflected
72 Kelvin wave become small, which may have significant impact on the El Niño-Southern
73 Oscillation (ENSO) variability in the Pacific Ocean.

74 Indeed, a recent study conducted by Jan et al. (2021) observed intraseasonal coastal sea
75 level oscillations off the west coast of Palawan (Fig. 1a and b) and hypothesized that the Rossby
76 waves partially penetrate the islands through Surigao Strait, a conduit between Philippine
77 marginal seas and the western Pacific Ocean at approximately 10°N, into Bohol and Sulu Seas to
78 the west of Palawan, and into central South China Sea (SCS). In addition to influences on the
79 dynamics, the potential penetration of Rossby waves may have substantial ecological impacts in
80 the southern Philippine archipelago via upwelling and mixing of nutrient-rich subsurface waters.
81 For example, Bohol Sea and Sulu Sea are important marginal seas in the Philippines with
82 significant coastal upwelling sites (Cabrera et al., 2011; Villanoy et al., 2011) that support
83 sardine fisheries. Additionally, the penetration of Rossby waves would elevate sea level

84 variations, amplifying the risk of severe damage during storm surges (Calafat et al., 2018). The
 85 potential ecological influences and the increased risk to extreme events warrant a comprehensive
 86 understanding of the characteristics of Rossby waves as they impinge on the eastern coasts of the
 87 Philippine archipelago from the east.

88 This study aims to examine the penetration of Rossby wave-induced sea level anomaly
 89 signals from the eastern to the western side of the Philippine archipelago and find their pathway
 90 and underlying physical processes. The satellite altimeter data and coastal tide gauge records are
 91 analyzed to clarify whether the relatively high sea level anomaly (> 0.2 m) observed in the east
 92 of the Philippines mainly originates from westward-propagating Rossby waves. Whether the
 93 waves could penetrate the southern Philippine islands and reach the SCS is also investigated,
 94 particularly for the fourth Rossby wave emanated from the west coast of Palawan observed by
 95 Jan et al. (2021). The results obtained from this study is expected to have important implications
 96 in many aspects, including climate dynamics, biogeochemical cycling of nutrients, and fisheries
 97 management within the Philippine waters.

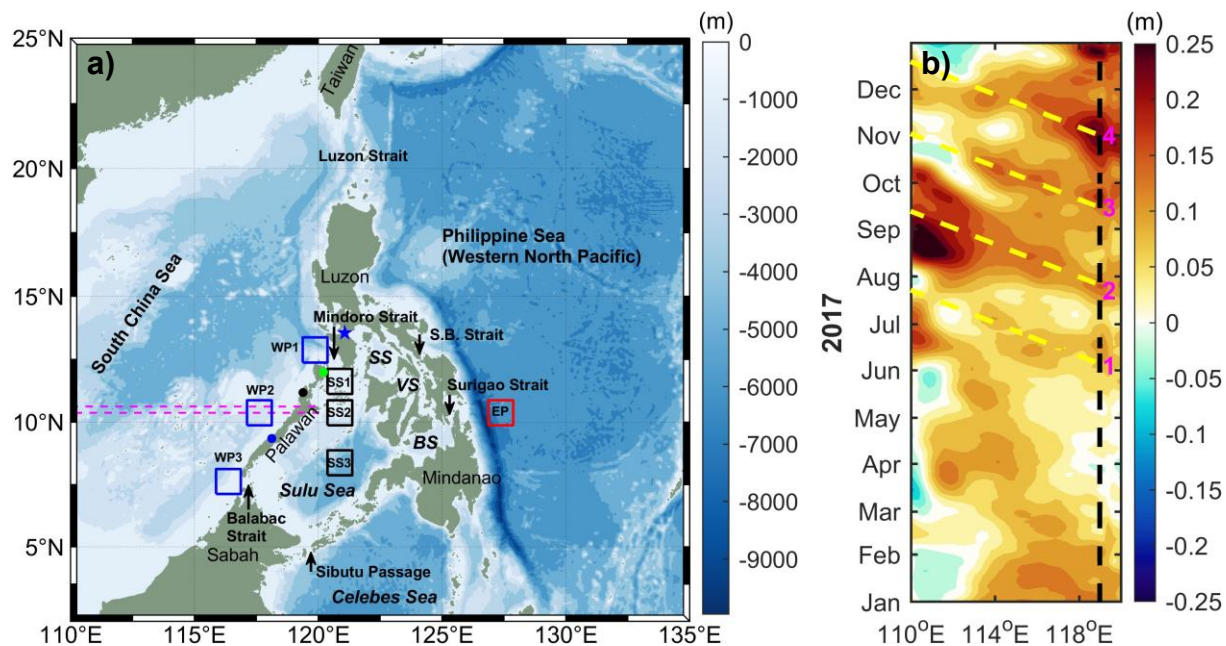


Fig. 1. (a) Bathymetric chart of the Philippine Sea and the South China Sea. Blue, black, and red boxes are the selected sites west of Palawan (WP1, WP2, and WP3), Sulu Sea (SS1, SS2, and SS3), and east of the Philippines (EP), respectively. Coastal tide gauge stations at Coron, El Nido, and Balintang are marked by green, black, and blue dots, respectively. A blue star marks Verde Island Passage. BS, VS, and SS are Bohol Sea, Visayan Sea, and Sibuyan Sea. The rectangle area enclosed by the magenta dashed lines is the meridionally-averaged satellite SLA used for depicting (b). (b) Hovmöller diagram (longitude vs. time) of satellite SLA at 10.5°N (Jan et al., 2021). The numerals 1–4 mark coastal sea level rise events occurring west of Palawan in 2017. Black dashed line indicates the west coast of Palawan. Yellow dashed lines indicate the westward-propagating SLA signals associated with events 1–4.

98 **2. Data and Methods**

99 2.1 Sea level data

100 The satellite altimeter-derived Global Ocean Gridded (L4) Sea Surface Heights and
101 Derived Variables Reprocessed provided by the Copernicus Marine Service (available at
102 <https://doi.org/10.48670/moi-00148>) were collected to identify Rossby waves in the context of
103 sea surface height observations. The satellite-derived sea level anomaly (SLA) data, with a
104 spatial resolution of 0.25° in both the north-south (meridional) and east-west (zonal) directions,
105 was computed by subtracting a 20-year (spanning from 1993 to 2012) mean sea level from the
106 original data covering the period 1993 to 2020. The processed SLAs were specifically examined,
107 particularly the year 2017, to validate the hypothesis raised by Jan et al. (2021) regarding the
108 penetration of Rossby waves through the Philippine islands. Sea level data recorded at three
109 coastal tide gauge stations (refer to Fig. 1b for their locations) were acquired from the National
110 Mapping and Resource Information Authority of the Philippines (<https://www.namria.gov.ph>) to
111 enhance the associated analysis.

112 2.1 Methodology

113 Whether a westward-propagating SLA signal can extend to the west of Palawan and into
114 the Philippine marginal seas, particularly in the Sulu Sea is the key to examine the transmission
115 of the signal through the Philippine islands. Time series of area-averaged daily SLA at seven
116 selected rectangles (Fig. 1a) are prepared for this purpose. Three of the seven selected sites are
117 located west of Palawan within the rectangle of 12.375° – 13.375° N and 119.375° – 120.375° E
118 (WP1), 9.875° – 10.875° N and 117.125° – 118.125° E (WP2), and 7.125° – 8.125° N and 115.875° –
119 116.875° E (WP3). The three sites located in the Sulu Sea are within the rectangle of 11.125° –
120 12.125° N and 120.375° – 121.375° E (SS1), 9.875° – 10.87° N and 120.375° – 121.375° E (SS2), and
121 7.875° – 8.875° N and 120.375° – 121.375° E (SS3). The last site is located east of the Philippines
122 (EP) bounded by 9.875° – 10.875° N and 126.875° – 127.875° E. The linear least-square fit of the
123 area-averaged daily SLA time series was subtracted from the original time series (Fig. 2a) to
124 eliminate trends in the data. In the tide-gauge station recorded sea levels, the data at Balintang
125 contains missing data (blue line in Fig. 2b), therefore a harmonic analysis based on Godin (1972)
126 and Foreman (1977, 1978) with the application of a MATLAB package T_Tide (Pawlowicz et

127 al., 2002) was used to compute the harmonic constants of the tidal sea levels at this station. The
 128 harmonic constants are subsequently used to composite the tidal sea level during the missing data
 129 period. Similar detrend method is applied to the tidal sea level records at the three Palawan
 130 stations.

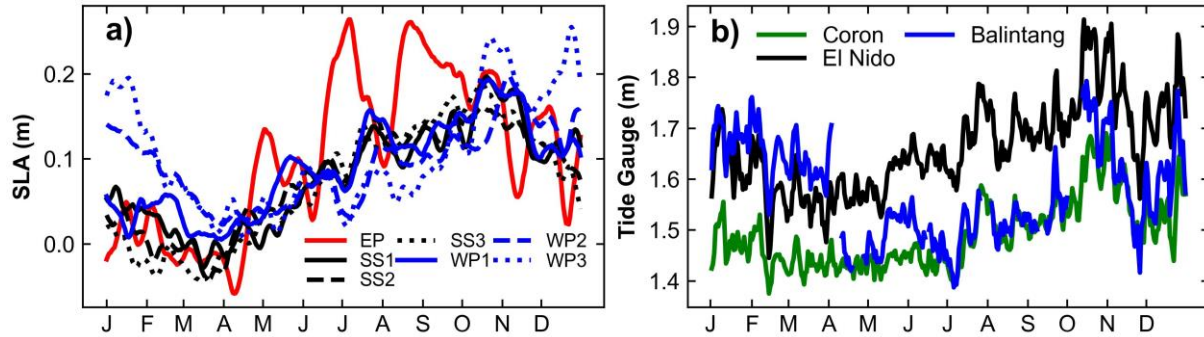


Fig. 2. (a) Time series of area-averaged daily SLA of the seven selected sites. (b) Time series of daily-averaged tide-gauge sea level records at the three Palawan stations.

131 The analysis involved examining monthly mean SLAs across the subtropical and tropical
 132 Pacific Ocean, spanning from 25°S to 25°N and from 110°E to 70°W. Signals of considerable
 133 magnitude, with absolute values > 0.2 m, were the focus of this analysis. A spatial low-pass filter
 134 achieved by an area mean of every 9×9 grids was applied to remove high-wavenumber features
 135 from the SLA maps (Fig. 3a–h). A Hovmöller diagram is plotted using the monthly mean SLA,
 136 meridionally averaged between 4.875° and 5.625°N, spanning across the Pacific Ocean from
 137 110°E to 70°W (Fig. 4a). The linear propagation speed of the SLA signal is estimated from the
 138 slope of each SLA signal (yellow dashed line in Fig. 4a). A wavelet power spectrum using
 139 Morlet wavelet is plotted using a 5-year (2015–2019) daily SLA average within the range of
 140 4.875°–5.625°N and 130°E–80°W (Fig. 4b) following the method of (Torrence & Compo,
 141 1998).

142 To quantify the characteristics of the Rossby waves, a wavenumber-frequency spectrum
 143 similar to the computation and illustration presented in Jan et al. (2021) is generated using a 20-
 144 year (2001–2020) daily SLA time series. The zonally SLA time series, spanning from 130°E to
 145 80°W, is the SLA average within the latitudinal band of 4.875° to 5.625°N (Fig. 4c and d). The
 146 dispersion relation of Rossby waves (red, yellow, and blue dashed lines in Fig. 4c and d) is
 147 computed using the equation (Cushman-Roisin, 1994),

148

$$\omega = -\beta_0 R^2 \frac{l}{1+R^2(l^2+m^2)},$$

149

150

151

152

153

154

155

156

157

158

159

where β_0 is the Rossby parameter defined as $\beta_0 = 2\Omega \cos\varphi a^{-1}$ (Ω is the angular velocity of the earth's rotation $7.2921 \times 10^{-5} \text{ rad s}^{-1}$, φ is the latitude 5°N here, and a is the earth's radius 6371 km), R is the Rossby radius of deformation, and l and m are zonal and meridional angular wavenumbers, respectively. The theoretical zonal phase speed (white lines in Fig. 4c and d) was calculated using $C_x = \omega/l$. The dispersion relation for baroclinic Rossby radius of deformation R 180, 215, and 260 km, is overlaid on the spectrum. The three radii are based on the globally computed first baroclinic Rossby radius of deformation climatology (Chelton et al., 1998) mean (± 1 standard deviation) within the range of $4.5^\circ\text{--}5.5^\circ\text{N}$ and $130^\circ\text{E--}80^\circ\text{W}$ $215.3 \pm 28.8 \text{ km}$. The wavenumber-frequency spectrum is used to examine the estimated Rossby wave speed and detect westward propagating SLA energy signals corresponding to that of the theoretical first baroclinic Rossby wave.

160

161

162

163

164

165

166

167

168

169

170

171

172

To detect the oscillation in an annual cycle, which is a characteristic of first baroclinic Rossby waves from $4^\circ\text{--}6^\circ\text{N}$ (Kessler, 1990; G. Meyers, 1979; Zang et al., 2002), the detrended SLA time series and tidal sea level records are low-pass filtered by applying a Butterworth filter with a cutoff frequency of $5.7870 \times 10^{-8} \text{ cps}$ (equivalent to 200-day period) to the time series data (Fig. 5a and b). To have a temporal and spatial view of the results obtained from Fig. 5b, the daily SLA in each grid ranging between $0^\circ\text{--}15^\circ\text{N}$ and $110^\circ\text{--}130^\circ\text{E}$ was detrended and low-pass filtered as the aforementioned procedure, and plotted as monthly mean as illustrated in Fig. 6a–i. Furthermore, a 30-day low-pass filter with a cutoff frequency of $3.8580 \times 10^{-7} \text{ cps}$ was applied to the detrended SLA time series and tidal sea level records. This processed SLA time series is used to clarify whether the observed SLA signal ($> 0.2 \text{ m}$) at 10.5°N east of the Philippines in Jan et al. (2021) was from a Rossby wave (Fig. 7a–d). The potential route of the Rossby wave penetration is also investigated. The monthly mean of low-pass-filtered SLAs within $0^\circ\text{--}15^\circ\text{N}$ and $110^\circ\text{--}180^\circ\text{E}$ are depicted in Fig. 8a–j.

173

3. Results and Discussion

174

3.1 Westward-propagating SLA signals

175

176

177

Fig. 3 shows the low-pass filtered monthly mean SLA over the tropical and subtropical Pacific Ocean. The filled blue (yellow) square and circle mark the center of the positive and negative SLA signals, respectively, in the northern (southern) hemisphere. The black (blue)

178 dashed line marks 5°N (6°S). Throughout the year 2017, noticeable basin-scale westward-
179 propagating positive and negative SLA signals were observed within the tropical Pacific band
180 ranging from 10°N to 10°S in both the northern and southern hemispheres. These SLA patterns
181 exhibit spatial and temporal characteristics consistent with Rossby waves, a finding supported by
182 analyses of satellite sea surface height observations (e.g., Chelton & Schlax, 1996; Zang et al.,
183 2002) and numerical model simulations (Fu et al., 1991; Spall & Pedlosky, 2005).

184 At 160°E (Fig. 3a), the positive SLA (crest) signifies downwelling, while at 165°W (Fig.
185 3d), the negative SLA (trough) indicates upwelling, which are the indicative pattern of Rossby
186 wave (Uz et al., 2001). These crest or trough pairs center around 5°N and 6°S , symmetrically
187 positioned concerning the equator. This alignment corresponds to the characteristic behavior of
188 the theoretical first meridional mode Rossby wave, initially proposed by Matsuno (1966) and
189 also agrees findings reported by Chelton and Schlax (1996), Delcroix et al. (1991), and Zang et
190 al. (2002), who utilized satellite-derived observations. Notably, Zang et al. (2002) observed
191 Rossby waves at 6°N and 6°S using TOPEX/Poseidon data spanning 1992–2000, differing
192 slightly from our findings of 5°N in the northern hemisphere. This difference in observed Rossby
193 wave locations may be attributed to variations in wind forcing. Kessler (1990) utilized
194 bathythermograph profiles in the northern tropical Pacific from 1970 to 1987 and found a close
195 resemblance between the amplitude pattern of wind stress curl, capable of generating Rossby
196 waves via Ekman pumping, and the depth of the 20°C isotherm (a proxy for sea surface height).
197 This similarity was particularly pronounced near $5\text{--}6^{\circ}\text{N}$, lending support to the observed location
198 of the Rossby wave noted by Zang et al. (2002) and this study. It is also worth noting that a
199 robust El Niño event occurred in 2015–2016, evidenced by the Ocean Niño Index (ONI)
200 reaching as high as 2.6 (NOAA/National Weather Service, 2023) prior to 2017. Given that
201 Rossby waves can manifest as a reflection of Kelvin waves upon reaching the eastern boundary
202 of the Pacific Ocean during El Niño events (Delcroix et al., 1994, 1991; Jacobs et al., 1994;
203 Kessler, 1990; McCreary, 1976), it is plausible that the Rossby wave observed in 2017 could
204 have originated from the 2015–2016 El Niño event.

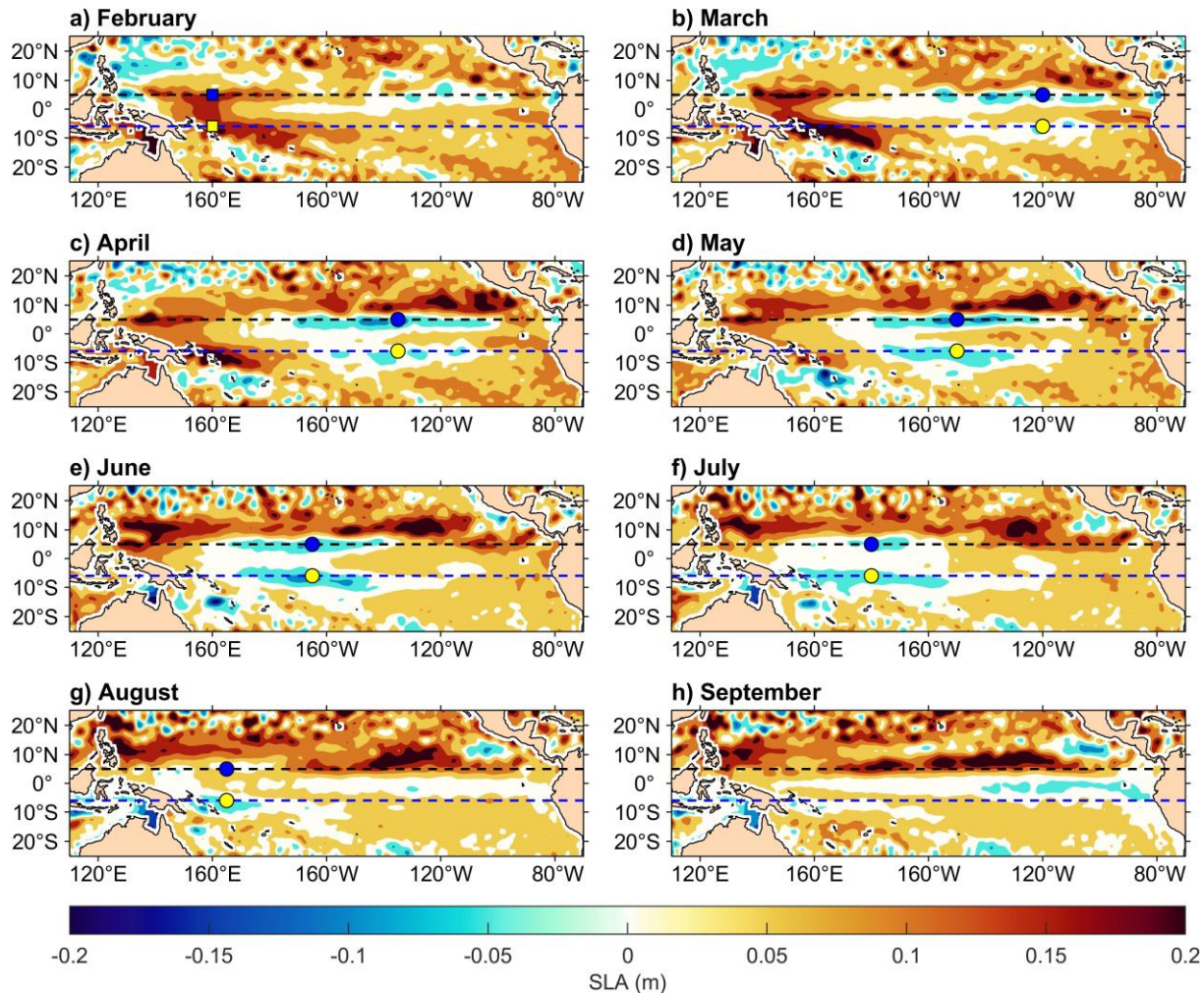


Fig. 3. Low-pass filtered satellite SLA in the subtropical and tropical Pacific Ocean. In the northern hemisphere (southern hemisphere), the filled blue (yellow) square and circle denote the centers of positive and negative SLA signals, respectively. The black dashed line represents 5°N , while the blue dashed line represents 6°S .

205 The monthly mean SLA depicted in Fig. 4a serves as the basis for calculating the phase
 206 speed of Rossby waves. These low-latitude SLA patterns observed in the northern hemisphere
 207 are anticipated to reach the east coast of the Philippines. Note that our analysis focuses on the
 208 prominent SLA signal, which manifests as a trough, indicated by the filled blue circles in Fig.
 209 3b–g. In the case of the crest, it had already translated halfway in the western boundary by April
 210 2017 (Fig. 3c), while the trough apparently propagated westward from March to July (Fig. 3b–f).
 211 The slope of the yellow dashed line in Fig. 4a corresponds to the phase speed of the Rossby
 212 wave, 0.64 m s^{-1} , at approximately 5°N . The wavelength of the Rossby wave is also estimated
 213 from Fig. 4a. The propagating distance of the crest between March and April (30 days) covered

214 15 degrees of longitude, marked by the filled yellow triangles in Fig. 4a, without considering
215 potential influences from a western boundary. In March, the Rossby wave crest and trough were
216 located at approximately 145°E and 120°W, respectively, which suggests a half wavelength of
217 ~10,545 km. Consequently, the estimated wavelength is 21,090 km. The associated period
218 estimated from Fig. 4a is approximately 12 months. Furthermore, from the wavelet power
219 spectrum of SLA in Fig. 4b illustrates SLA energy predominantly in 2017, with a period of 360
220 days.

221 The wavenumber-frequency spectrum depicted in Fig. 4c reveals the presence of energy
222 attributed to a basin-scale westward-propagating SLA with an annual period. This energy aligns
223 closely with the dispersion relation computed using baroclinic Rossby radii of 180 km
224 (illustrated by the red dashed line) and 260 km (shown as the blue dashed line) in Fig. 4c. Upon
225 magnifying the area enclosed by the black rectangle in Fig. 4d (corresponding to Fig. 4c), the
226 period associated with relatively low SLA energy (enclosed by the black oval) falls within the
227 range of 350 to 360 days. The SLA energy, close to the dispersion relation computed with a 180
228 km radius of deformation, exhibits a theoretical phase speed of approximately -0.7 m s^{-1} (the
229 negative sign implies westward propagation) and a wavenumber of approximately $-4.5 \times 10^{-8} \text{ m}^{-1}$
230 (or ~22,000 km). These values are comparable to the characteristics of the Rossby wave
231 observed in 2017. These findings are consistent with those reported by Kessler (1990) of a
232 Rossby wave near 5°N which exhibited an annual period, a zonal wavelength of ~23,000 km
233 (model estimate ~21,000 km), and a model-derived phase speed of $\sim 0.67 \text{ m s}^{-1}$.

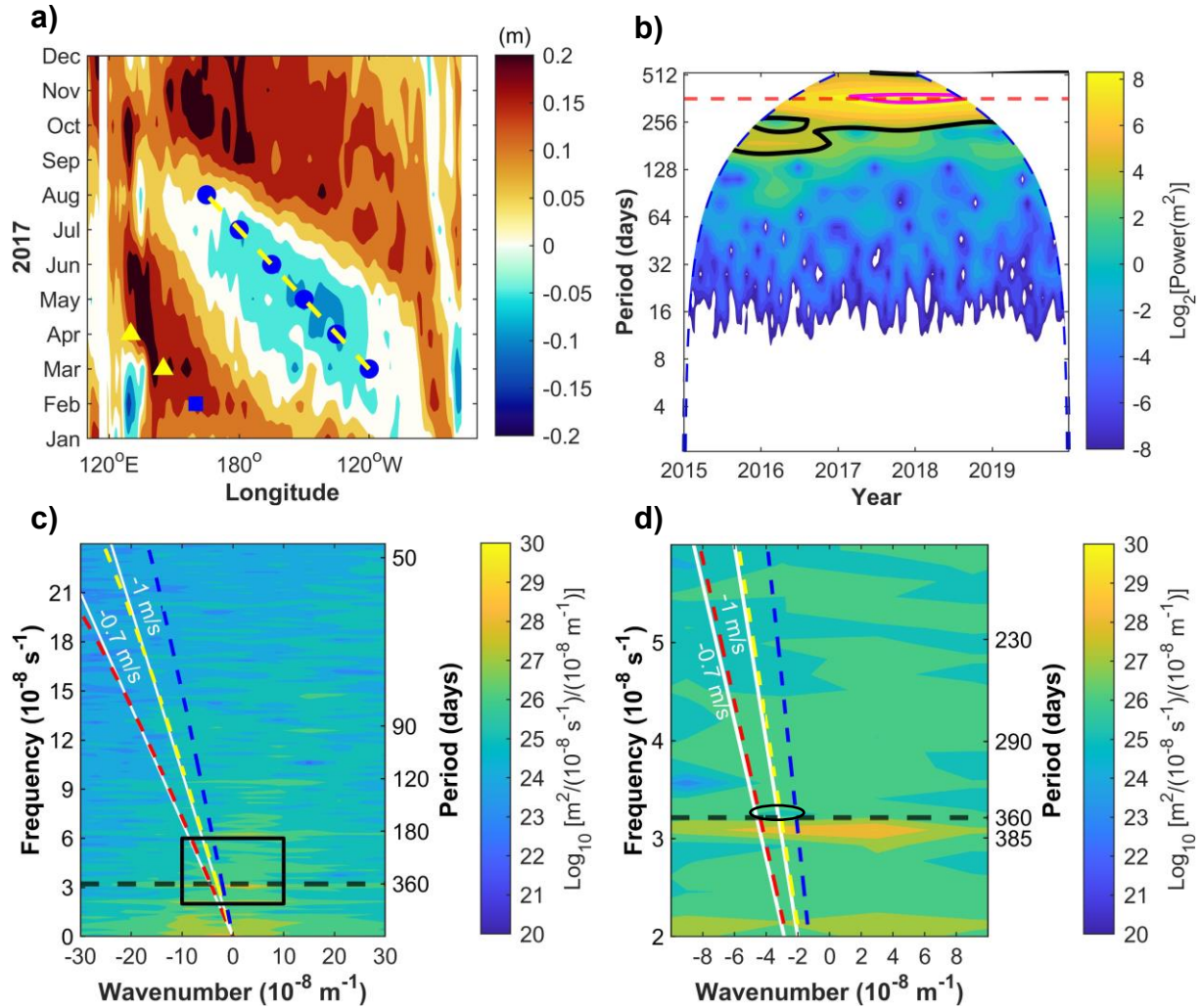


Fig. 4. (a) Hovmöller diagram illustrating satellite-derived SLA centered at 5°N . The filled blue square and circle correspond to those in Fig. 2a–g. The filled yellow triangles denote the crest centers in March and April, with the yellow dashed line indicating the phase speed of the westward-propagating negative SLA signal. (b) Wavelet power spectrum normalized by corresponding variance ($\sigma^2 = 0.0015 \text{ m}^2$). The blue dashed line indicates the cone of influence. The red dashed line denotes the 360-day period. Magenta contour is the SLA energy with approximately annual period. Black contour indicates the region with greater than 95% confidence level. (c) Wavenumber-frequency spectrum of satellite SLA. The red, yellow, and blue dashed lines are dispersion relations computed using R of 180, 215, and 260 km, respectively. The white lines show the computed theoretical phase speeds of -0.7 and -1 m s^{-1} . The horizontal black dashed line marks 360 days. (d) A close-up of the black rectangle in (c), where the black oval indicates westward-propagating (negative wavenumber) SLA energy with periods within 350 and 360 days.

234 3.2 Penetration of SLA signals through the Celebes Sea

235 Fig. 5 shows detrended and 200-day low-pass filtered satellite SLA time series off the
236 eastern Philippines (red line), in the Sulu Sea (black lines), and off the west coast of Palawan
237 (blue lines). In Fig. 5a, detrended and 200-day low-pass filtered sea level data from tide gauge
238 stations (cyan lines) are presented for comparative analysis. The low-frequency sea level
239 variations observed at WP2 (blue dashed line) and WP3 (blue dotted line) off the west coast of
240 Palawan show significant correlation with those recorded at Balintang (cyan dotted line),
241 exhibiting Pearson's correlation coefficients of 0.90 and 0.95, respectively. Moreover, WP2
242 exhibits a strong correlation with sea level variations at Coron (cyan line) and El Nido (cyan
243 dashed line), with correlation coefficients of 0.97 and 0.88, respectively. This finding suggests
244 that the satellite-derived SLA within these specific areas can effectively serve as a proxy for
245 understanding coastal sea level variations along the west coast of Palawan.

246 Further to the north, the low-frequency sea level variation at WP1 (blue line) and SS1
247 (black line) show relatively weak (correlation coefficient 0.36) and moderate (correlation
248 coefficient 0.60) correlations, respectively, with those observed at Coron (cyan line).
249 Importantly, the low-frequency sea level variation at SS1 exhibit a notably high correlation
250 (correlation coefficient 0.90) with El Nido (cyan dashed line). This finding supports that the
251 long-term variability of SLA at the major passage connecting the Sulu Sea and the SCS, the
252 Mindoro Strait, can be effectively assessed using satellite altimeter data. Therefore, the analysis
253 of detrended and low-pass filtered satellite-derived SLA proves pivotal in examining the
254 potential penetration of Rossby waves and understanding their probable pathway.

255 Fig. 5b shows that a quasi-annual sea level oscillation with period > 330 days extending
256 from February to December 2017 is clearly observed at WP2 and WP3. At WP2, the crest higher
257 than 2 cm (filled red) appears during April–May, while a trough lower than -2 cm (blue shading)
258 is noticeable during August and October. A similar pattern can be observed at WP3 but with
259 relatively higher amplitude (> 3 cm for crest and < -3 cm for trough).

260 The annual variation of SLAs at SS2 and SS3 in the Sulu Sea have similar magnitudes to
261 that at WP1 with a crest approximately 1 cm (green shading) and a trough lower than -2 cm
262 (magenta shading) around March–April and July, respectively. Note that SS1 has relatively
263 higher amplitude with a crest higher than 1 cm (brown shading) in April and a trough lower than
264 -3 cm (yellow shading) in August. The low-frequency satellite SLA at EP does not exhibit a

265 similar oscillatory pattern observed in the 2017 Rossby wave observed at $\sim 5^\circ\text{N}$. This is
 266 presumably due to the more northerly location of EP ($\sim 10^\circ\text{N}$), affecting the distinctive
 267 characteristics observed at this latitude.

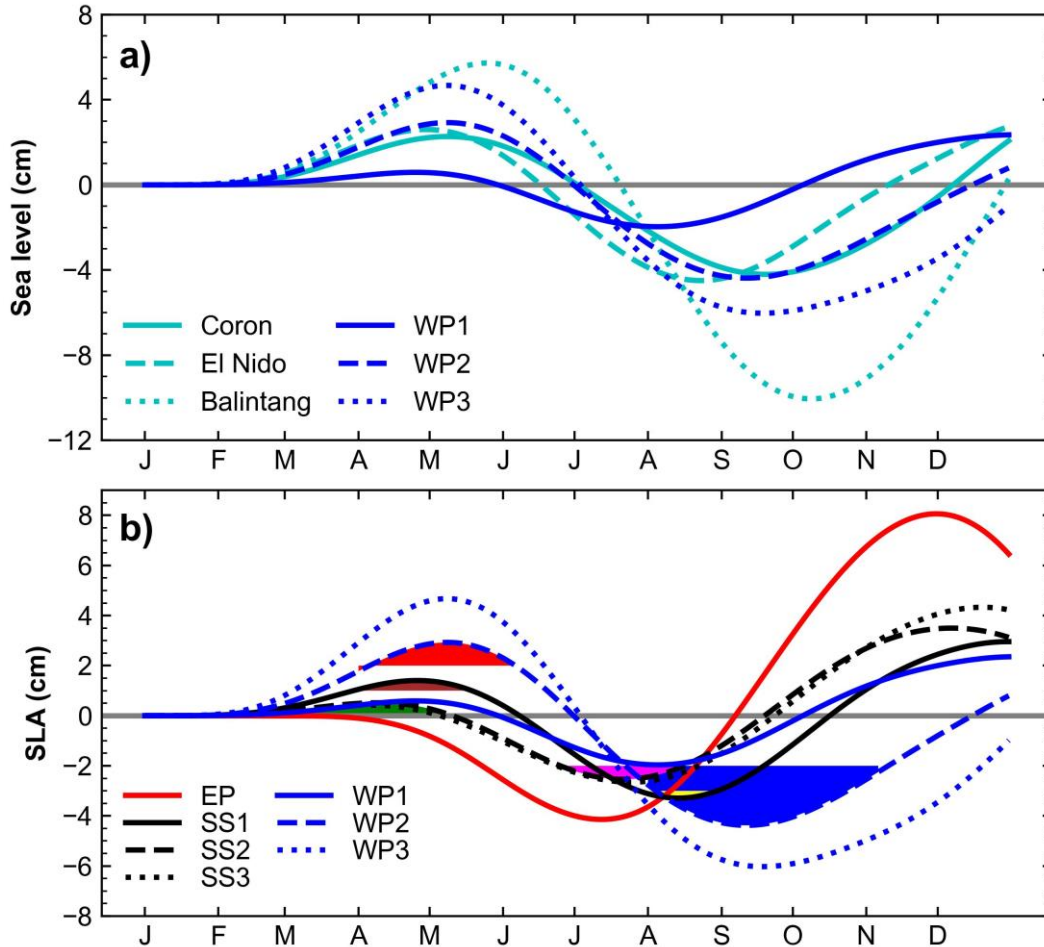


Fig. 5. (a) Time series of detrended and 200-day low-pass filtered satellite SLA and tide gauge station recorded sea levels west and north of Palawan. (b) Detrended and 200-day low-pass filtered satellite SLA across Philippines. Red and blue shadings indicate satellite SLA greater than 2 cm and lower than -2 cm, respectively, at WP2. Green and magenta shadings are satellite SLA smaller than 1 cm and lower than -2 cm, respectively, at SS2 and SS3. Brown and yellow shadings are satellite SLA greater than 1 cm and lower than -3 cm, respectively, at SS1.

268 The cross-correlation (correlation coefficient r_{SLA}) of the low-frequency satellite SLA
 269 between SS2 and EP is 0.96 at zero-lag. At WP2 and SS1, WP2 and SS2, and WP2 and WP1, the
 270 r_{SLA} is 0.77 at a 27-day lag, 0.51 at a 54-day lag, and 0.63 at a 37-day lag, respectively.
 271 Analyzing the variability of the low-pass filtered SLAs in Fig. 5b reveals that the crest (green

272 shading) and trough (magenta shading) occurrences in the northern Sulu Sea (SS2) lead those off
273 the west coast of Palawan at WP2 (red and blue shading in Fig. 5b) by 54 days.

274 This result suggests that the SLA oscillation at WP2 could be sourced from the northern
275 Sulu Sea via the Mindoro Strait. The lagged correlation between EP and SS2, however, suggests
276 that no physically plausible SLA signal penetrated from the east of the Philippines through the
277 Surigao Strait (see its location in Fig. 1a) to the Sulu Sea (SS2). The most plausible entrance of
278 the associated SLA signal is the Sibutu Passage (Fig. 1a), which connects the Celebes and Sulu
279 Seas. Results from the lagged cross-correlation analysis further suggest that, after entering Sibutu
280 Passage, the low-frequency SLA oscillation moved from SS2 to SS1 toward the Mindoro Strait
281 in the Sulu Sea. After passing through the Mindoro Strait into the central SCS, the coherent SLA
282 signal moved southward along the west coast of Palawan.

283 The pathway of the transmitted SLA signal is examined using the low-pass filtered
284 satellite SLA around the Philippine archipelago (Fig. 6a–i). In March 2017, positive SLA of
285 approximately 2 cm appeared off the west coast of Palawan, in the Sulu Sea, and the southern
286 part of the Celebes Sea (Fig. 6a). The positive SLA continuously increased to greater than 2 cm
287 in these regions and northeast of Sabah in April and May (Fig. 6b and c). As time progressed to
288 June, the SLA along the east and northern half coast of Palawan decreased to smaller than 2 cm,
289 while the southern half coast of Palawan and the southern Celebes Sea remained larger than 2 cm
290 (Fig. 6d). The SLA eventually diminished in July (Fig. 6e). The SLA pattern dramatically
291 reversed from positive to negative in August (Fig. 6f). Thereafter the SLA over these regions
292 remained negative until November (Fig. 6g–i).

293 The aforementioned results suggest that the penetration of the 2017 Rossby wave is
294 plausible, particularly for the SLA crest. It indicates that the Rossby wave transmitted into the
295 Celebes Sea at about 5°N in March (Fig. 3b). As the Rossby wave further entered the Sulu Sea
296 through the Sibutu Passage, it went along the northeast coast of Sabah and the east coast of
297 Palawan through Mindoro Strait and between Coron and El Nido. After the SLA signal passed
298 the Mindoro Strait to the SCS, SLA signal extended to the west coast of Palawan (Fig. 6d). Note
299 that a relatively higher SLA signal (> 4 cm) appeared south of Palawan, which suggests that the
300 SLA signal could also transmit through the narrow and shallow Balabac Strait. It is also noticed
301 that the SLA signal (> 2 cm) expanded to the Makassar Strait connecting the Celebes Sea and the
302 Java Sea (Fig. 6c), which is indicative of the Rossby wave transmitting toward the Indonesian

303 marginal seas as well as the Indian Ocean (du Penhoat and Cane, 1991; Spall and Pedlosky,
 304 2005). The temporal and spatial patterns of the negative SLA signal (Rossby wave trough in Fig.
 305 6f-i) are similar to those of the positive SLA signal.

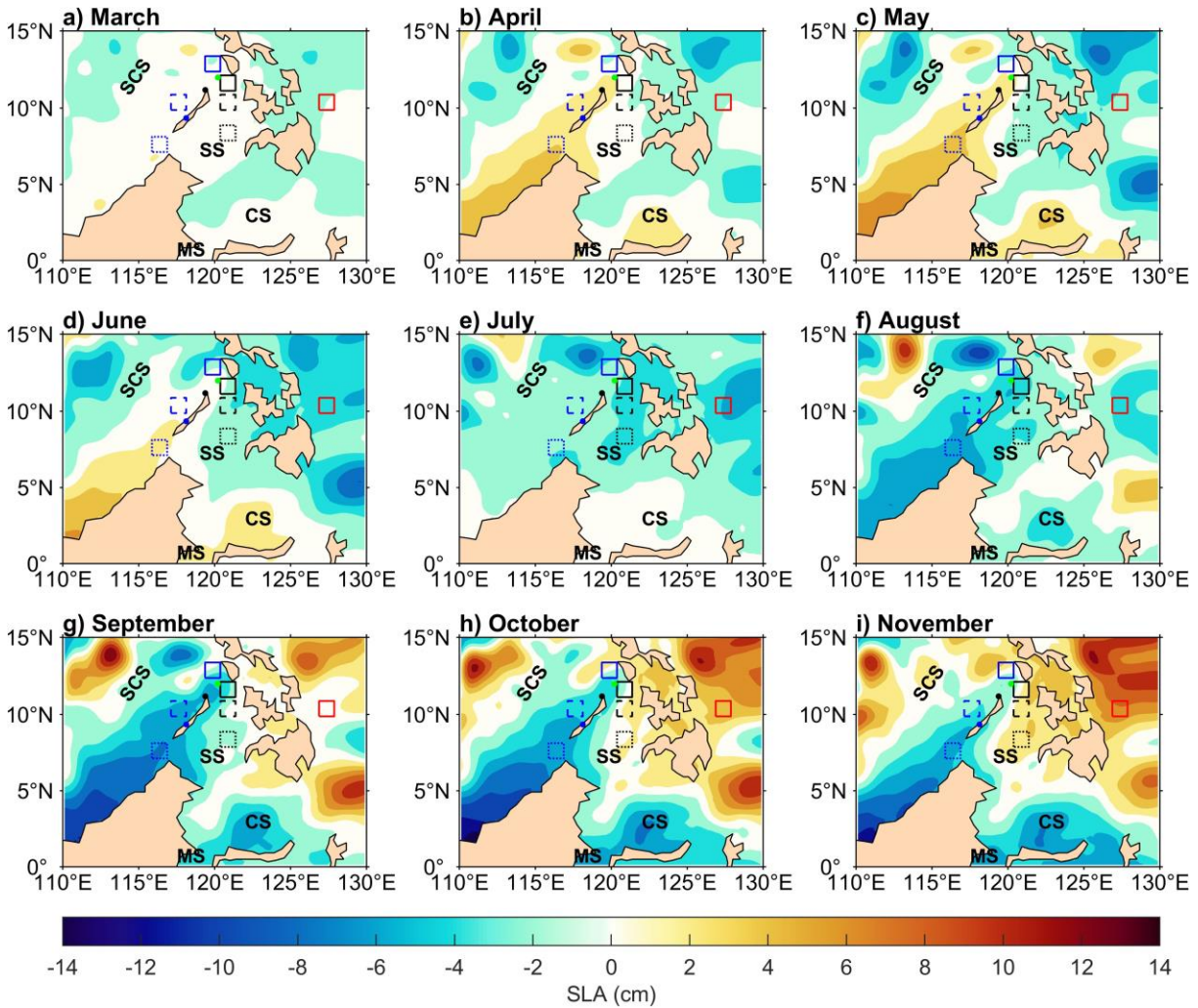


Fig. 6. Monthly mean of temporal and spatial variation in detrended and 200-day low-pass filtered satellite SLA around the Philippines. The color and line style of the rectangles correspond to those in Fig. 4b. CS means Celebes Sea, SS represents Sulu Sea, SCS represents South China Sea, and MS stands for Makassar Strait.

306 3.3 Penetration of SLA signals through Surigao Strait

307 Fig. 7 shows the detrended and 30-day low-pass filtered satellite SLA and tide gauge
 308 record time series. In the west of Palawan, this processed SLA at WP2 (blue dashed line) and
 309 WP3 (blue dotted line) are highly correlated with that at Balintang (cyan dotted line) and their
 310 correlation coefficients are 0.70 and 0.82, respectively, as the processed SLA at WP1 (blue line)

311 is highly correlated with that at El Nido (cyan dashed line) with a correlation coefficients of 0.75.
312 In the northern part of Sulu Sea, the SLA at SS1 (black line) is highly correlated with the tide
313 gauge sea level at Coron (cyan line) and El Nido (cyan dashed line), and the correlation
314 coefficients are 0.75 and 0.90, respectively. Fig. 7b–d show the SLA time series east of
315 Philippines (EP), Sulu Sea (SS1–SS3), and west of Palawan (WP1–WP3). Noticeable peaks with
316 the processed SLA greater than 10 cm appeared in the middle of July and early September 2017
317 at EP. In the Sulu Sea, SLA peaks (4–6 cm) appeared in early August and early November. West
318 of the Palawan, SLA peaks (6–10 cm) were also in early August (at WP1 only) and early
319 November (at WP1 and WP3), whereas SLA peaks at WP2 (2–6 cm) appeared in mid-August
320 and late November, which are approximately 10 days behind that of WP1. The period of
321 significant SLA oscillation (amplitude > 10 cm) at EP was during July and October (thick
322 vertical black dashed lines in Fig. 7b–d). Whereas at SS1, SS2, and WP1, the period was from
323 August to November. Additionally, significant SLA oscillation at WP2 (thin vertical black dash
324 lines in Fig. 7d), was from early August to early December, which is approximately 10 days after
325 that at SS1, SS2, and WP1.

326 The r_{SLA} of satellite SLA at SS1, SS2, and SS3 versus that of EP are 0.66 at 20-day lag,
327 0.70 at 20-day lag, and 0.73 at 15-day lag, respectively. The r_{SLA} between WP2 and WP1, SS1,
328 and SS2 is 0.60 at 10-day lag, 0.70 at 8-day lag, and 0.41 at 16-day lag, respectively. These
329 suggest that the associated SLA signal at EP leads that in the Sulu Sea, and the signal in the Sulu
330 Sea leads that off west of Palawan at approximately 20 and 10 days, respectively. The period of
331 significant SLA oscillations and lagged correlations suggest that the SLA off the eastern
332 Philippines leads that in the Sulu Sea and in turn the west of Palawan, particularly at WP2.

333 The aforementioned SLA analysis supports the hypothesis proposed by Jan et. al. (2021),
334 which suggests the penetration of Rossby waves through the Philippine archipelago to the Bohol
335 and Sulu Seas and exiting Mindoro Strait (WP1) and Balabac Strait (WP3) to the west of
336 Palawan (WP2). The Rossby waves eventually emanated from the west coast of Palawan
337 propagating westward in the central SCS. This could be the source of the fourth intraseasonal
338 velocity and satellite oscillations off Palawan and explains the weak correlation of the fourth
339 event of southwesterly monsoon strengthening during early October 2017 and the SLA rise along
340 the west coast of Palawan in November (Jan et al., 2021).

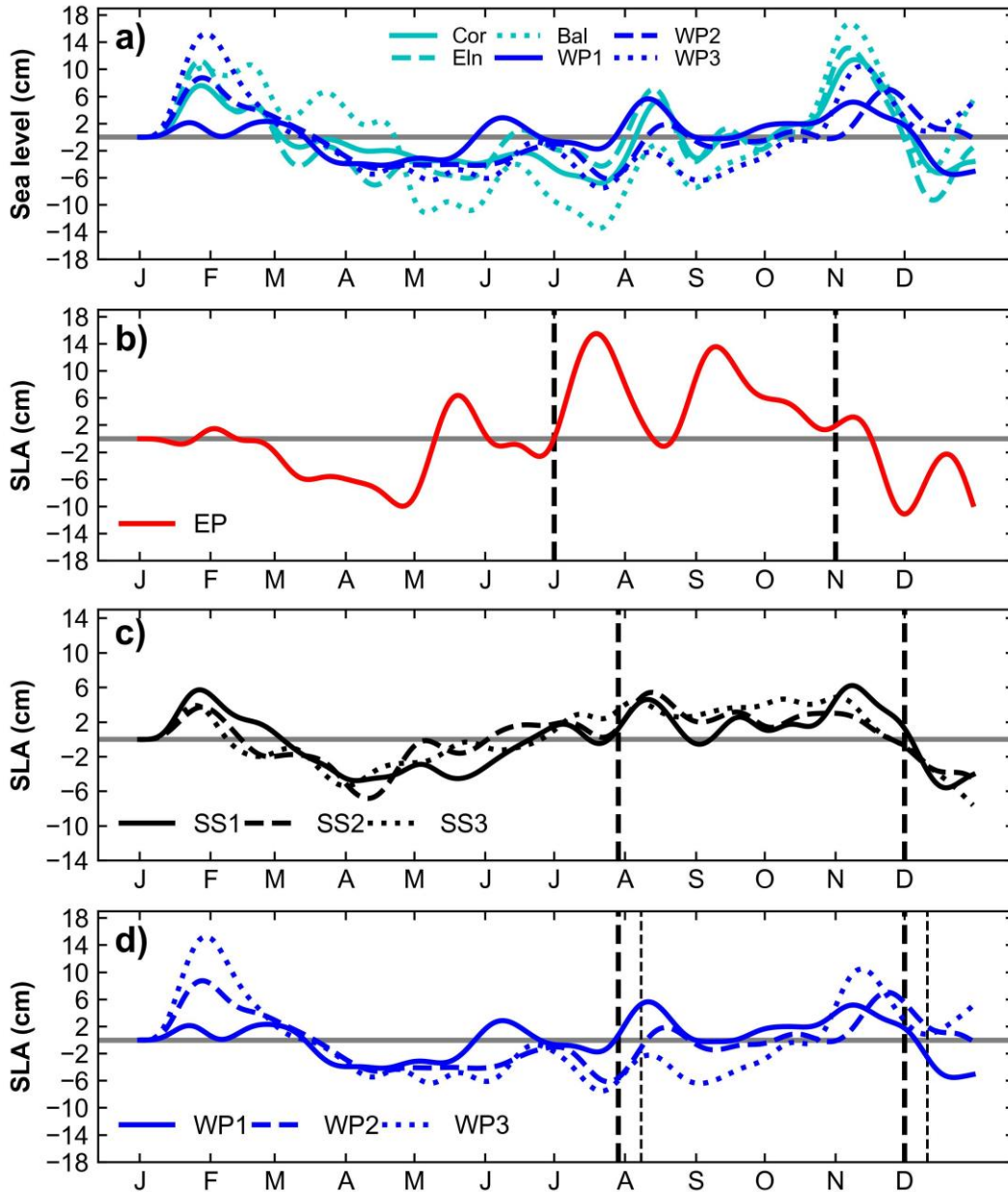


Fig. 7. (a) Time series of detrended and 30-day low-pass filtered satellite SLA alongside tide gauge station recorded sea levels west and north of Palawan. Detrended and 30-day low-pass filtered satellite SLA at (b) EP, (c) S1–S3, and (d) WP1–WP3. Thick vertical black dashed lines indicate the duration of positive SLA signal (crest). Thin vertical black dashed lines indicate the duration of positive SLA signal (crest) in WP2.

341 The peaks in the SLA variations observed east of the Philippines is verified using the
 342 temporal and spatial variations of processed SLA from the SCS to the 180°E (Fig. 8a–j). The
 343 westward-propagating positive and negative SLA signals at approximately 5°N impinged on the
 344 western boundary from April to October (Fig. 8b–h). These SLA signals observed in Fig. 3a–g

345 are verified as the first baroclinic Rossby wave, which penetrated the southern Philippine
346 archipelago (Fig. 6) and induced a quasi-annual oscillation off the west coast of Palawan (Fig. 5).
347 Between approximately 10° and 15°N , westward-propagating positive and negative SLA signals
348 impinged on the western boundary from July to December (Fig. 8e–j). These SLA signals show
349 characteristics of beta-refracted Rossby waves as those observed by Chelton and Schlax (1996)
350 and Jacobs et al. (1994). The beta-refracted Rossby waves are generated by the reflection of
351 Kelvin waves along the eastern boundary (Jacobs et al., 1994; Sirven et al., 2019). In the case we
352 analyzed, the boundary is the western coastlines of the central and north America. The wave
353 speed estimated using time-longitude plot of detrended and 30-day low-pass filtered daily SLA
354 centered at 10.5°N (i.e., 10.375° – 10.625°N average) from 130°E – 180° is approximately 0.28 m
355 s^{-1} (Figure S1), which is comparable to the first mode of baroclinic Rossby waves wave speed
356 0.2 – 0.3 m s^{-1} at about 10.5°N obtained from the theory (Chelton and Schlax, 1996) and the
357 observation (Jan et al., 2021).

358 The possible pathways of the beta-refracted Rossby wave crest transmitted across the
359 Philippine archipelago is examined using Fig. 8e–i. In July (Fig. 8e), the crest impinged on the
360 eastern Philippines, which resulted in a SLA peak greater than 10 cm east of the Philippines (Fig.
361 7b), and entered the Surigao Strait (see Fig. 1a). One month later, in August (Fig. 8f), the crest
362 progressed into the Sulu Sea via Bohol Sea and into the northern Palawan via Bohol Sea,
363 Visayan Sea, Sibuyan Sea, and Mindoro Strait, as shown by the simultaneous peaks of
364 approximately 6 cm at S1–S3 (Fig. 7c) and WP1 (Fig. 7d). Subsequently, this SLA peak moved
365 toward WP2 with approximately 2 cm height 10 days after passed WP1 (Fig. 7d). The 2 cm peak
366 at WP2 propagated westward, contributed to the second event (Fig. 1b) observed by Jan et al.
367 (2021), and consequently resulted in a decrease in SLA at WP2 (Fig. 8g and 7d) in September.
368 The trailing crest continued to propagate toward WP2 in October (Fig. 8h) and November (Fig.
369 8i). In November, the SLA crest (Fig. 8i) apparently passed WP1 (Mindoro Strait) and WP3
370 (Balabac Strait) led to a 6 cm and 8 cm peaks in early November (Fig. 7d), respectively. This
371 SLA signal eventually reached WP2 (Fig. 7d) and further propagated westward as the fourth
372 event in Fig. 1b (Jan et al., 2021). Note that the Rossby wave crest (Fig. 8e–g) at approximately
373 13°N could also pass San Bernardino Strait (S.B. Strait in Fig. 1a), Sibuyan Sea, and exit
374 Mindoro Strait and Verde Island Passage (blue star in Fig. 1a).

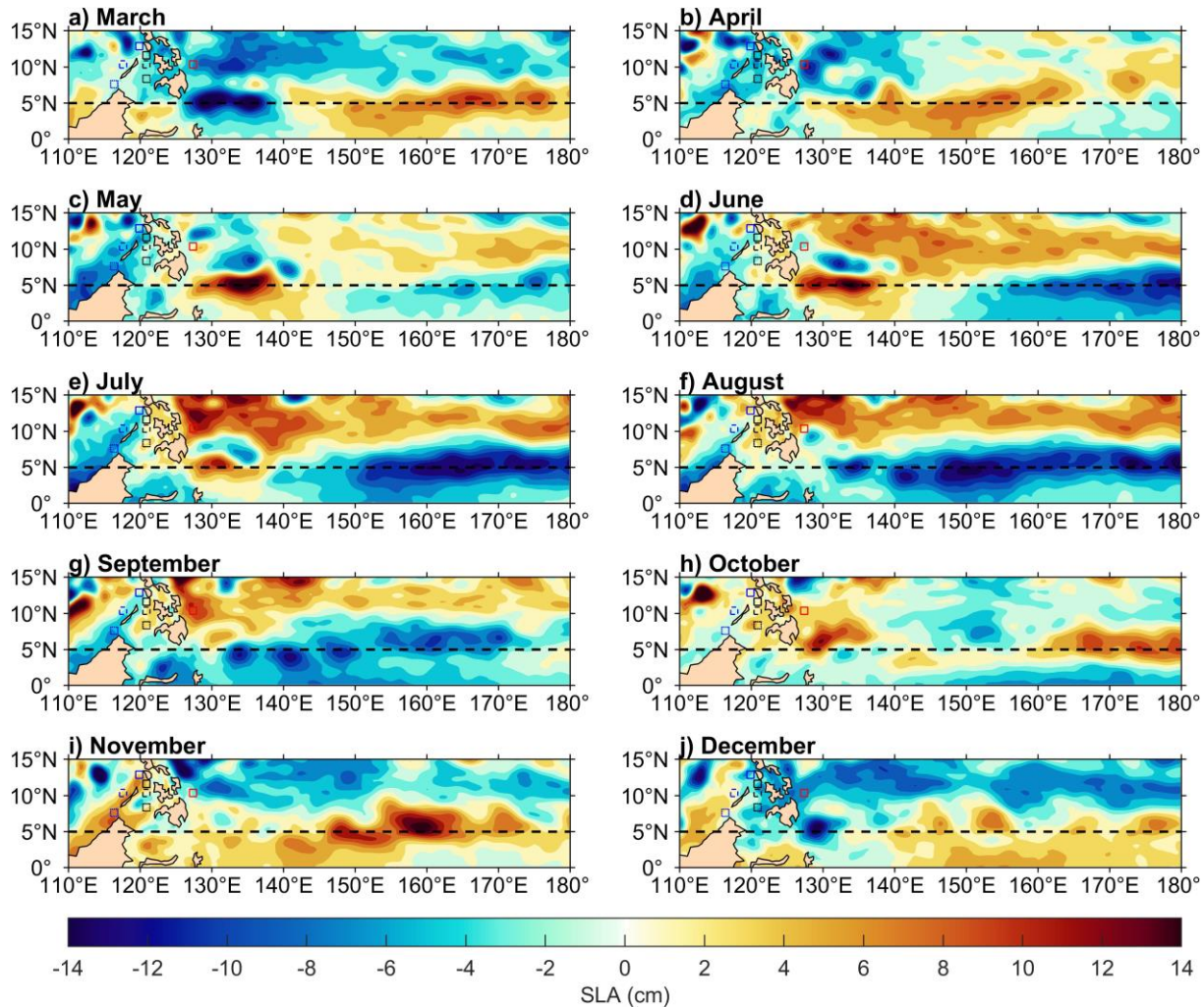


Fig. 8. Monthly temporal and spatial variations in detrended and 30-day low-pass filtered satellite SLA. The color and line style of the rectangles correspond to those presented in Fig. 7b–d.

375 4. Conclusions

376 The examination of satellite-derived SLA data, combined with sea level information
 377 gathered from fixed tide gauge stations along the Philippine coasts, delineated the westward
 378 propagation of first baroclinic Rossby waves within the tropical Pacific Ocean. This analysis
 379 revealed these waves' potential to transmit the southern Philippine archipelago and penetrate into
 380 the SCS. The estimated wave speed for the Rossby wave is approximately 0.64 m s^{-1} , exhibiting
 381 a wavelength of $\sim 21,000 \text{ km}$ and a yearly period. This wave speed is comparable to that of the
 382 Rossby waves at about 5°N , which is 0.7 m s^{-1} obtained from the theory and $\sim 0.67 \text{ m s}^{-1}$ derived
 383 from the numerical simulation (Kessler, 1990).

384 Notably, among the Rossby waves detected from satellite SLA data between 2015 and
385 2019, the 2017 Rossby wave emerged as the most prominent. This particular Rossby wave
386 translated westward along 5°N , reaching the western boundary of the North Pacific before
387 entering the Celebes Sea and proceeding into the Sulu Sea via the Sibutu Passage. The indicative
388 SLA signal of the Rossby wave hugged the northeast coast of Sabah and east coast of Palawan,
389 and passed through the Mindoro Strait and the passage between Coron and El Nido to the west of
390 Palawan. As the schematic shown in Fig. 9, the Rossby wave also passed the Makassar Strait,
391 potentially extending its influence into the Indian Ocean.

392 The temporal progression of the SLA around the Mindoro Strait also suggests that a pair
393 of cyclonic and anticyclonic eddies could be generated when the flow generated by the Rossby
394 wave passed westward through the Mindoro Strait. In addition to these findings, a β -refracted
395 Rossby wave, positioned at approximately 10.5°N , is observed with wave speed of 0.28 m s^{-1} ,
396 which is close to the theoretical speed of 0.25 m s^{-1} (Chelton & Schlax, 1996) and observed
397 speed of $0.2\text{--}0.3\text{ m s}^{-1}$ (Jan et al., 2021). The crest of this β -refracted Rossby wave impinged on
398 the east coast of the Philippines and penetrated through the archipelago through the Surigao
399 Strait. As illustrated by Fig. 8, two pathways toward west of Palawan are observed: one directed
400 southward to the Bohol Sea, Sulu Sea, and Balabac Strait and the other translated northward to
401 the Bohol Sea, Visayan Sea, Sibuyan Sea, and Mindoro Strait of Palawan island.

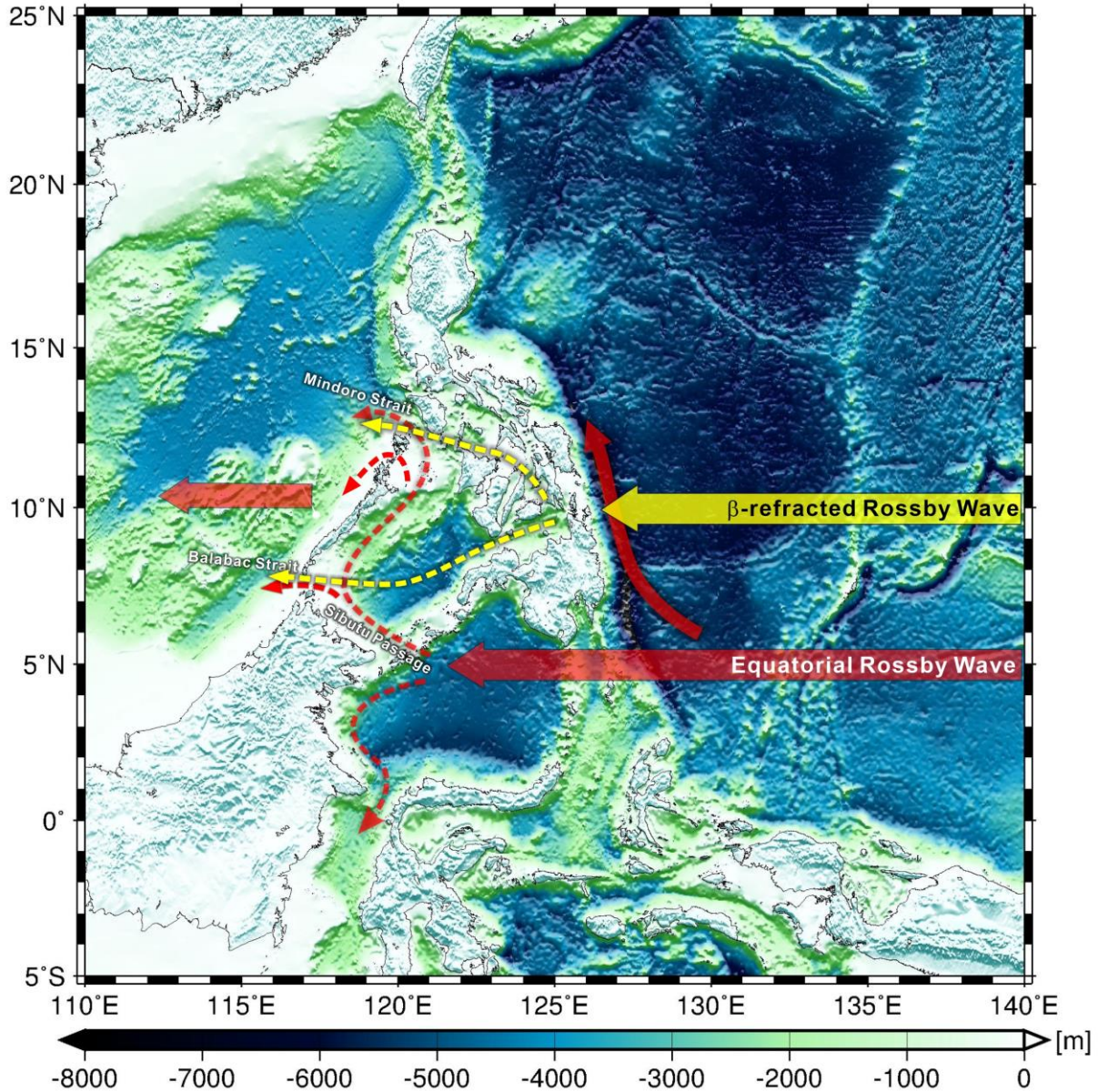


Fig. 9. A schematic diagram showing the transmission routes of both westward-propagating equatorial and β -refracted Rossby waves.

402 **Acknowledgments**

403 Yi-Chen Cheng and Yu-Yu Yeh helped plot the bathymetry chart and wavenumber-
 404 frequency spectrum, respectively. To NAMRIA Administrator Peter N. Tiangco for the hourly
 405 coastal sea level data products. This work was supported by the National Science and
 406 Technology Council (NSC) of Taiwan. SJ is sponsored under grant NSC-111-2611-M-002-020,

407 NSC-111-2119-M-002-014, and NSTC-112-2119-M-002-023. MEDM is sponsored under grant
408 NSTC-112-2119-M-002 -023. TYH is sponsored by the NSTC.

409

410 **Data Availability Statement**

411 Satellite SLA is obtained from CMEMS (accessible at <https://doi.org/10.48670/moi-00148>). Sea level records from tide gauge stations in Palawan is available at
412 <https://doi.org/10.5281/zenodo.10396727>.
413

414

415 **References**

416 Anderson, D. L. T., Bryan, K., Gill, A. E., & Pacanowski, R. C. (1979). The transient response
417 of the North Atlantic: Some model studies. *Journal of Geophysical Research*, 84(C8), 4795.
418 <https://doi.org/10.1029/JC084iC08p04795>

419 Anderson, D. L. T., & Gill, A. E. (1975). Spin-up of a stratified ocean, with applications to
420 upwelling. *Deep Sea Research and Oceanographic Abstracts*, 22(9), 583–596.
421 [https://doi.org/10.1016/0011-7471\(75\)90046-7](https://doi.org/10.1016/0011-7471(75)90046-7)

422 Cabanes, C., Huck, T., & Colin de Verdière, A. (2006). Contributions of Wind Forcing and
423 Surface Heating to Interannual Sea Level Variations in the Atlantic Ocean. *Journal of
424 Physical Oceanography*, 36(9), 1739–1750. <https://doi.org/10.1175/JPO2935.1>

425 Cabrera, O. C., Villanoy, C. L., David, L. T., & Gordon, A. L. (2011). Barrier layer control of
426 entrainment and Upwelling in the Bohol Sea, Philippines. *Oceanography*, 24(1), 130–141.
427 <https://doi.org/10.5670/oceanog.2011.10>

428 Calafat, F. M., Wahl, T., Lindsten, F., Williams, J., & Frajka-Williams, E. (2018). Coherent
429 modulation of the sea-level annual cycle in the United States by Atlantic Rossby waves.
430 *Nature Communications*, 9(1). <https://doi.org/10.1038/s41467-018-04898-y>

431 Chelton, D. B., deSzoeko, R. A., Schlax, M. G., El Naggar, K., & Siwertz, N. (1998).
432 Geographical Variability of the First Baroclinic Rossby Radius of Deformation. *Journal of
433 Physical Oceanography*, 28(3), 433–460. [https://doi.org/10.1175/1520-0485\(1998\)028<0433:GVOTFB>2.0.CO;2](https://doi.org/10.1175/1520-0485(1998)028<0433:GVOTFB>2.0.CO;2)

435 Chelton, D. B., & Schlax, M. G. (1996). Global Observations of Oceanic Rossby Waves.
436 *Science*, 272(5259), 234–238. <https://doi.org/10.1126/science.272.5259.234>

- 437 Cushman-Roisin, B., & Beckers, J.-M. (2011). Chapter 9 - Barotropic waves, in International
438 Geophysics, edited by B. Cushman-Roisin and J.-M. Beckers, pp. 271–315, Academic
439 Press, <https://doi.org/10.1016/B978-0-12-088759-0.00009-2>.
- 440 Delcroix, T., Picaut, J., & Eldin, G. (1991). Equatorial Kelvin and Rossby waves evidenced in
441 the Pacific Ocean through Geosat sea level and surface current anomalies. *Journal of*
442 *Geophysical Research*, *96*(S01), 3249. <https://doi.org/10.1029/90JC01758>
- 443 du Penhoat, Y., & Cane, M. A. (1991). Effect of low-latitude western boundary gaps on the
444 reflection of equatorial motions. *Journal of Geophysical Research*, *96*(S01), 3307.
445 <https://doi.org/10.1029/90jc01798>
- 446 Foreman, M.G.G. (1977). Manual for tidal heights analysis and prediction. *Pacific Marine*
447 *Science Report 77-10*, Institute of Ocean Sciences, Patricia Bay, Sidney, British Columbia.
- 448 Foreman, M.G.G. (1978). Manual for tidal currents analysis and prediction. *Pacific Marine*
449 *Science Report 78-6*, Institute of Ocean Sciences, Patricia Bay, Sidney, British Columbia.
- 450 Fu, L.-L., Vazquez, J., & Perigaud, C. (1991). Fitting Dynamic Models to the Geosat Sea Level
451 Observations in the Tropical Pacific Ocean. Part I: A Free Wave Model. *Journal of Physical*
452 *Oceanography*, *21*(6), 798–809. [https://doi.org/10.1175/1520-](https://doi.org/10.1175/1520-0485(1991)021<0798:FDMTTG>2.0.CO;2)
453 [0485\(1991\)021<0798:FDMTTG>2.0.CO;2](https://doi.org/10.1175/1520-0485(1991)021<0798:FDMTTG>2.0.CO;2)
- 454 Godin, G. (1991). The analysis of tides and currents. In: Parker, B.B. (Ed.), *Tidal*
455 *Hydrodynamics*. New York: Wiley.
- 456 Jacobs, G. A., Emery, W. J., & Born, G. H. (1993). Rossby Waves in the Pacific Ocean
457 Extracted from Geosat Altimeter Data. *Journal of Physical Oceanography*, *23*(6), 1155–
458 1175. [https://doi.org/10.1175/1520-0485\(1993\)023<1155:RWITPO>2.0.CO;2](https://doi.org/10.1175/1520-0485(1993)023<1155:RWITPO>2.0.CO;2)
- 459 Jacobs, G. A., Hurlburt, H. E., Kindle, J. C., Metzger, E. J., Mitchell, J. L., Teague, W. J., &
460 Wallcraft, A. J. (1994). Decade-scale trans-Pacific propagation and warming effects of an
461 El Niño anomaly. *Nature*, *370*(6488), 360–363. <https://doi.org/10.1038/370360a0>
- 462 Jan, S., Chang, M. H., Yang, Y. J., Sui, C. H., Cheng, Y. H., Yeh, Y. Y., & Lee, C. W. (2021).
463 Mooring observed intraseasonal oscillations in the central South China Sea during summer
464 monsoon season. *Scientific Reports*, *11*(1). <https://doi.org/10.1038/s41598-021-93219-3>
- 465 Kessler, W. S. (1990). Observations of long Rossby waves in the northern tropical Pacific.
466 *Journal of Geophysical Research*, *95*(C4), 5183–5217.
467 <https://doi.org/10.1029/JC095iC04p05183>

- 468 Matsuno, T. (1966). Quasi-Geostrophic Motions in the Equatorial Area. *Journal of the*
469 *Meteorological Society of Japan. Ser. II, 44(1), 25–43.*
470 https://doi.org/10.2151/jmsj1965.44.1_25
- 471 McCreary, J. (1976). Eastern Tropical Ocean Response to Changing Wind Systems: with
472 Application to El Niño. *Journal of Physical Oceanography, 6(5), 632–645.*
473 [https://doi.org/10.1175/1520-0485\(1976\)006<0632:ETORTC>2.0.CO;2](https://doi.org/10.1175/1520-0485(1976)006<0632:ETORTC>2.0.CO;2)
- 474 Meyers, G. (1979). Annual Variation in the Slope of the 14°C Isotherm along the Equator in the
475 Pacific Ocean. *Journal of Physical Oceanography, 9(5), 885–891.*
476 [https://doi.org/10.1175/1520-0485\(1979\)009<0885:AVITSO>2.0.CO;2](https://doi.org/10.1175/1520-0485(1979)009<0885:AVITSO>2.0.CO;2)
- 477 Meyers, S. D., Liu, M., O'Brien, J. J., Johnson, M. A., & Spiesberger, J. L. (1996). Interdecadal
478 Variability in a Numerical Model of the Northeast Pacific Ocean: 1970–89. *Journal of*
479 *Physical Oceanography, 26(12), 2635–2652.* [https://doi.org/10.1175/1520-](https://doi.org/10.1175/1520-0485(1996)026<2635:IVIANM>2.0.CO;2)
480 [0485\(1996\)026<2635:IVIANM>2.0.CO;2](https://doi.org/10.1175/1520-0485(1996)026<2635:IVIANM>2.0.CO;2)
- 481 National Oceanic and Atmospheric Administration, National Weather Service, Climate
482 Prediction Center. (2023). Cold and warm episodes by season. Retrieved from
483 https://origin.cpc.ncep.noaa.gov/products/analysis_monitoring/ensostuff/ONI_v5.php
- 484 Pawlowicz, R., Beardsley, B., & Lentz, S. (2002). Classical tidal harmonic analysis including
485 error estimates in MATLAB using T_TIDE. *Computers & Geosciences, 28(8), 929–937.*
486 [https://doi.org/10.1016/S0098-3004\(02\)00013-4](https://doi.org/10.1016/S0098-3004(02)00013-4)
- 487 Piecuch, C. G., & Ponte, R. M. (2012). Buoyancy-driven interannual sea level changes in the
488 southeast tropical Pacific. *Geophysical Research Letters, 39(5).*
489 <https://doi.org/10.1029/2012GL051130>
- 490 Qiu, B. (2003). Kuroshio Extension Variability and Forcing of the Pacific Decadal Oscillations:
491 Responses and Potential Feedback. *Journal of Physical Oceanography, 33(12), 2465–2482.*
492 <https://doi.org/10.1175/2459.1>
- 493 Sirven, J., Mignot, J., & Crépon, M. (2019). Generation of Rossby waves off the Cape Verde
494 Peninsula: The role of the coastline. *Ocean Science, 15(6), 1667–1690.*
495 <https://doi.org/10.5194/os-15-1667-2019>
- 496 Spall, M. A., & Pedlosky, J. (2005). Reflection and Transmission of Equatorial Rossby Waves*.
497 *Journal of Physical Oceanography, 35(3), 363–373.* <https://doi.org/10.1175/JPO-2691.1>

- 498 Stammer, D., Park, S., Köhl, A., Lukas, R., & Santiago-Mandujano, F. (2008). Causes for large-
499 scale hydrographic changes at the Hawaii Ocean time series station. *Journal of Physical*
500 *Oceanography*, 38(9), 1931–1948. <https://doi.org/10.1175/2008JPO3751.1>
- 501 Torrence, C., & Compo, G. P. (1998). A Practical Guide to Wavelet Analysis. *Bulletin of the*
502 *American Meteorological Society*, 79(1), 61–78. [https://doi.org/10.1175/1520-](https://doi.org/10.1175/1520-0477(1998)079<0061:APGTWA>2.0.CO;2)
503 [0477\(1998\)079<0061:APGTWA>2.0.CO;2](https://doi.org/10.1175/1520-0477(1998)079<0061:APGTWA>2.0.CO;2)
- 504 Uz, B. M., Yoder, J. A., & Osychny, V. (2001). Pumping of nutrients to ocean surface waters by
505 the action of propagating planetary waves. *Nature*, 409(6820), 597–600.
506 <https://doi.org/10.1038/35054527>
- 507 Villanoy, C. L., Cabrera, O. C., Yñiguez, A., Camoying, M., de Guzman, A., David, L. T., &
508 Lament, P. F. (2011). Monsoon-driven coastal upwelling off Zamboanga peninsula,
509 Philippines. *Oceanography*, 24(1), 156–165. <https://doi.org/10.5670/oceanog.2011.12>
- 510 White, W. B. (2000). Tropical Coupled Rossby Waves in the Pacific Ocean–Atmosphere
511 System. *Journal of Physical Oceanography*, 30(6), 1245–1264.
512 [https://doi.org/10.1175/1520-0485\(2000\)030<1245:TCRWIT>2.0.CO;2](https://doi.org/10.1175/1520-0485(2000)030<1245:TCRWIT>2.0.CO;2)
- 513 White, W. B., Chao, Y., & Tai, C.-K. (1998). Coupling of Biennial Oceanic Rossby Waves with
514 the Overlying Atmosphere in the Pacific Basin. *Journal of Physical Oceanography*, 28(6),
515 1236–1251. [https://doi.org/10.1175/1520-0485\(1998\)028<1236:COBORW>2.0.CO;2](https://doi.org/10.1175/1520-0485(1998)028<1236:COBORW>2.0.CO;2)
- 516 Zang, X., Fu, L. L., & Wunsch, C. (2002). Observed reflectivity of the western boundary of the
517 equatorial Pacific Ocean. *Journal of Geophysical Research: Oceans*, 107(10).
518 <https://doi.org/10.1029/2000jc000719>
519

Transmission of Rossby waves through the Philippine Archipelago

Mac Euan D. Malugao^{1,2,5}, Sen Jan³, Ming-Huei Chang³, Tung-Yuan Ho^{1,3,4}, Yiing Jang Yang³

¹ Earth System Science Program, Taiwan International Graduate Program, Academia Sinica, Taipei, Taiwan, R.O.C.

² Taiwan International Graduate Program for Earth System Science, National Taiwan University, Taipei, Taiwan, R.O.C.

³ Institute of Oceanography, National Taiwan University, Taipei, Taiwan, R.O.C.

⁴ Research Center for Environmental Changes, Academia Sinica, Taipei, Taiwan, R.O.C.

⁵ Department of Marine Science, College of Science and Mathematics, Mindanao State University – Iligan Institute of Technology, Iligan City, Philippines

Corresponding author: Sen Jan (senjan@ntu.edu.tw)

Key Points:

- Satellite altimeter proved Rossby wave transmission through the Philippine archipelago and into central South China Sea.
- Rossby waves entered Celebes Sea and passed Sibutu Passage into Sulu Sea, while β -refracted Rossby wave entered Sulu Sea via Surigao Strait.
- The Mindoro Strait and the Balabac Strait served as gateways for the Rossby waves entering the central South China Sea from the Sulu Sea.

22 **Abstract**

23 Oceanic Rossby waves play a crucial role in shaping the physical and biological
24 dynamics of both open and coastal oceans, especially within the tropical band spanning between
25 the 10°S and 10°N parallels. Yet, the extent to which Rossby waves can transmit and impact the
26 hydrography and ecosystem of semi-enclosed seas like the South China Sea (SCS) remains
27 unclear. This study aims to investigate the transmission of Rossby waves through the Philippine
28 archipelago, using satellite altimeter-derived sea level anomaly (SLA) and coastal tide gauge
29 records. Our findings reveal that westward-propagating Rossby waves in the tropical Pacific
30 Ocean with a wave speed of $\sim 0.64 \text{ m s}^{-1}$ first entered the Celebes Sea, and then passed through
31 the Sibutu Passage into the Sulu Sea from April to December 2017. Subsequently, the waves
32 propagated along the northeast coast of Sabah and the east coast of Palawan before exiting
33 through the Mindoro Strait to the central SCS. Additionally, a β -refracted Rossby wave with
34 wave speed of 0.28 m s^{-1} also penetrated the archipelago but at a latitude further north $\sim 10^\circ\text{N}$
35 from July to November via Surigao Strait and propagated toward the south and north of Palawan,
36 ultimately reaching the west coast of Palawan in the eastern central SCS. This study verifies that
37 the transmission of Rossby waves originating from the east of the Philippines could induce
38 intraseasonal sea level oscillations off Palawan, which could subsequently propagate westward
39 across the central SCS as identified in previous field observations.

40

41 **Keywords:** Sea level anomaly, satellite altimeter, Hovmöller diagram, first baroclinic mode,
42 western boundary

43 **Plain Language Summary**

44 Oceanic Rossby waves are like movers shaping how things work in the world's oceans,
45 especially in tropical bands between 10 degrees south and 10 degrees north of the equator. We
46 wanted to figure out how these waves travel and affect seas like the South China Sea. Using data
47 from satellites and measurements along the coast, we discovered that these waves, traveling at
48 about 0.64 meters per second, first went through the Celebes Sea, then moved through specific
49 passages to reach the Sulu Sea between April and December 2017. Another type of Rossby wave
50 traveled at a different speed through a different route, arriving at the same destination in the
51 South China Sea. This research helps us understand how these waves move through the
52 Philippine islands and impact sea levels around them.

53 **1. Introduction**

54 Large-scale westward-propagating oceanic Rossby waves, which can be identified from
55 sea level anomalies observed by satellites, significantly impact the sea surface height variations,
56 geostrophic current, and hydrography in the ocean and the weather and climate from the
57 atmospheric variations during their journey across the entire basin (Chelton & Schlax, 1996;
58 Jacobs et al., 1993). They transport heat in the meridional direction, regulate the climate,
59 redistribute the water mass and nutrients in the ocean, and shape the ocean circulation (e.g.,
60 Anderson & Gill, 1975; Jacobs et al., 1994; Meyers et al., 1996; Stammer et al., 2008; Uz et al.,
61 2001; White et al., 1998). The formation of Rossby waves may originate from wind burst forcing
62 (Anderson et al., 1979; Cabanes et al., 2006; Qiu, 2003), the reflection of Kelvin waves in the
63 eastern boundary (Delcroix et al., 1991; Jacobs et al., 1994; McCreary, 1976), or buoyancy
64 forcing (Piecuch & Ponte, 2012). As Rossby waves approach the western boundary, they can
65 intensify the western boundary current (Anderson et al., 1979; Anderson & Gill, 1975), modulate
66 local sea-level annual cycles (Calafat et al., 2018), and reflect from the western boundary to form
67 Kelvin waves propagating eastward along the equator (du Penhoat & Cane, 1991; White, 2000;
68 Zang et al., 2002). In addition to their importance in ocean dynamics, du Penhoat and Cane
69 (1991) and Spall and Pedlosky (2005) suggested that, as a first mode baroclinic Rossby wave
70 impinges on a small meridional gap in the western boundary, a considerable portion of incident
71 wave energy can transmit through the gap, while wave energy and, in turn, amplitude of reflected
72 Kelvin wave become small, which may have significant impact on the El Niño-Southern
73 Oscillation (ENSO) variability in the Pacific Ocean.

74 Indeed, a recent study conducted by Jan et al. (2021) observed intraseasonal coastal sea
75 level oscillations off the west coast of Palawan (Fig. 1a and b) and hypothesized that the Rossby
76 waves partially penetrate the islands through Surigao Strait, a conduit between Philippine
77 marginal seas and the western Pacific Ocean at approximately 10°N, into Bohol and Sulu Seas to
78 the west of Palawan, and into central South China Sea (SCS). In addition to influences on the
79 dynamics, the potential penetration of Rossby waves may have substantial ecological impacts in
80 the southern Philippine archipelago via upwelling and mixing of nutrient-rich subsurface waters.
81 For example, Bohol Sea and Sulu Sea are important marginal seas in the Philippines with
82 significant coastal upwelling sites (Cabrera et al., 2011; Villanoy et al., 2011) that support
83 sardine fisheries. Additionally, the penetration of Rossby waves would elevate sea level

84 variations, amplifying the risk of severe damage during storm surges (Calafat et al., 2018). The
 85 potential ecological influences and the increased risk to extreme events warrant a comprehensive
 86 understanding of the characteristics of Rossby waves as they impinge on the eastern coasts of the
 87 Philippine archipelago from the east.

88 This study aims to examine the penetration of Rossby wave-induced sea level anomaly
 89 signals from the eastern to the western side of the Philippine archipelago and find their pathway
 90 and underlying physical processes. The satellite altimeter data and coastal tide gauge records are
 91 analyzed to clarify whether the relatively high sea level anomaly (> 0.2 m) observed in the east
 92 of the Philippines mainly originates from westward-propagating Rossby waves. Whether the
 93 waves could penetrate the southern Philippine islands and reach the SCS is also investigated,
 94 particularly for the fourth Rossby wave emanated from the west coast of Palawan observed by
 95 Jan et al. (2021). The results obtained from this study is expected to have important implications
 96 in many aspects, including climate dynamics, biogeochemical cycling of nutrients, and fisheries
 97 management within the Philippine waters.

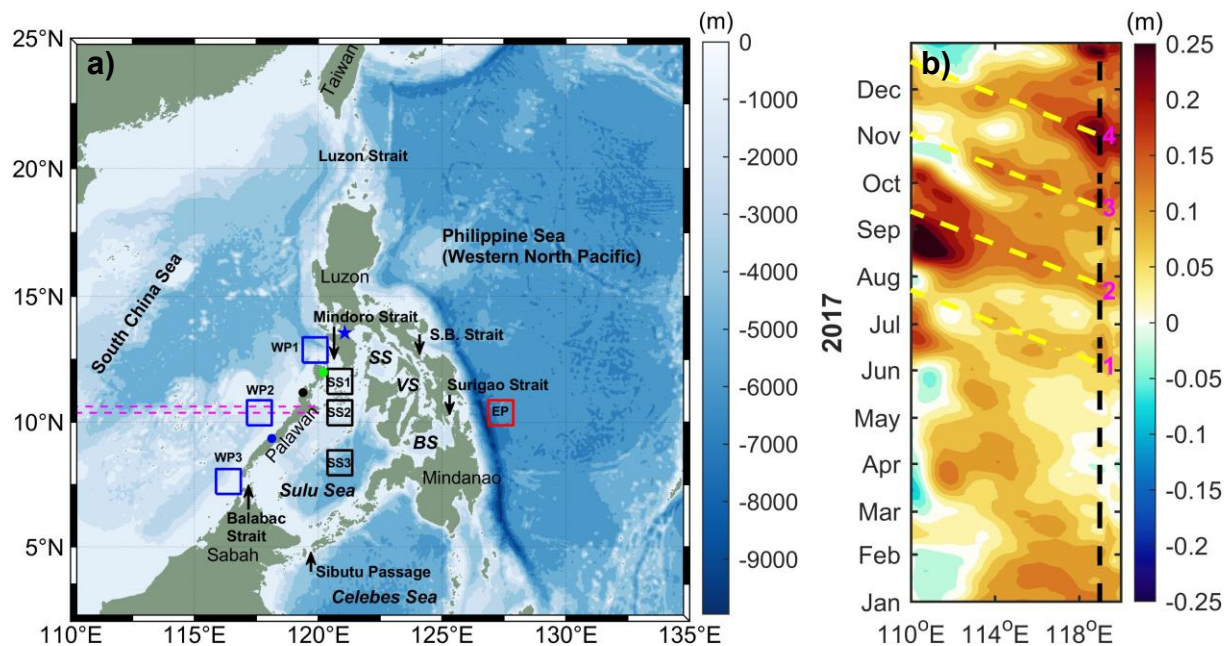


Fig. 1. (a) Bathymetric chart of the Philippine Sea and the South China Sea. Blue, black, and red boxes are the selected sites west of Palawan (WP1, WP2, and WP3), Sulu Sea (SS1, SS2, and SS3), and east of the Philippines (EP), respectively. Coastal tide gauge stations at Coron, El Nido, and Balintang are marked by green, black, and blue dots, respectively. A blue star marks Verde Island Passage. BS, VS, and SS are Bohol Sea, Visayan Sea, and Sibuyan Sea. The rectangle area enclosed by the magenta dashed lines is the meridionally-averaged satellite SLA used for depicting (b). (b) Hovmöller diagram (longitude vs. time) of satellite SLA at 10.5°N (Jan et al., 2021). The numerals 1–4 mark coastal sea level rise events occurring west of Palawan in 2017. Black dashed line indicates the west coast of Palawan. Yellow dashed lines indicate the westward-propagating SLA signals associated with events 1–4.

98 **2. Data and Methods**

99 2.1 Sea level data

100 The satellite altimeter-derived Global Ocean Gridded (L4) Sea Surface Heights and
101 Derived Variables Reprocessed provided by the Copernicus Marine Service (available at
102 <https://doi.org/10.48670/moi-00148>) were collected to identify Rossby waves in the context of
103 sea surface height observations. The satellite-derived sea level anomaly (SLA) data, with a
104 spatial resolution of 0.25° in both the north-south (meridional) and east-west (zonal) directions,
105 was computed by subtracting a 20-year (spanning from 1993 to 2012) mean sea level from the
106 original data covering the period 1993 to 2020. The processed SLAs were specifically examined,
107 particularly the year 2017, to validate the hypothesis raised by Jan et al. (2021) regarding the
108 penetration of Rossby waves through the Philippine islands. Sea level data recorded at three
109 coastal tide gauge stations (refer to Fig. 1b for their locations) were acquired from the National
110 Mapping and Resource Information Authority of the Philippines (<https://www.namria.gov.ph>) to
111 enhance the associated analysis.

112 2.1 Methodology

113 Whether a westward-propagating SLA signal can extend to the west of Palawan and into
114 the Philippine marginal seas, particularly in the Sulu Sea is the key to examine the transmission
115 of the signal through the Philippine islands. Time series of area-averaged daily SLA at seven
116 selected rectangles (Fig. 1a) are prepared for this purpose. Three of the seven selected sites are
117 located west of Palawan within the rectangle of 12.375° – 13.375° N and 119.375° – 120.375° E
118 (WP1), 9.875° – 10.875° N and 117.125° – 118.125° E (WP2), and 7.125° – 8.125° N and 115.875° –
119 116.875° E (WP3). The three sites located in the Sulu Sea are within the rectangle of 11.125° –
120 12.125° N and 120.375° – 121.375° E (SS1), 9.875° – 10.87° N and 120.375° – 121.375° E (SS2), and
121 7.875° – 8.875° N and 120.375° – 121.375° E (SS3). The last site is located east of the Philippines
122 (EP) bounded by 9.875° – 10.875° N and 126.875° – 127.875° E. The linear least-square fit of the
123 area-averaged daily SLA time series was subtracted from the original time series (Fig. 2a) to
124 eliminate trends in the data. In the tide-gauge station recorded sea levels, the data at Balintang
125 contains missing data (blue line in Fig. 2b), therefore a harmonic analysis based on Godin (1972)
126 and Foreman (1977, 1978) with the application of a MATLAB package T_Tide (Pawlowicz et

127 al., 2002) was used to compute the harmonic constants of the tidal sea levels at this station. The
 128 harmonic constants are subsequently used to composite the tidal sea level during the missing data
 129 period. Similar detrend method is applied to the tidal sea level records at the three Palawan
 130 stations.

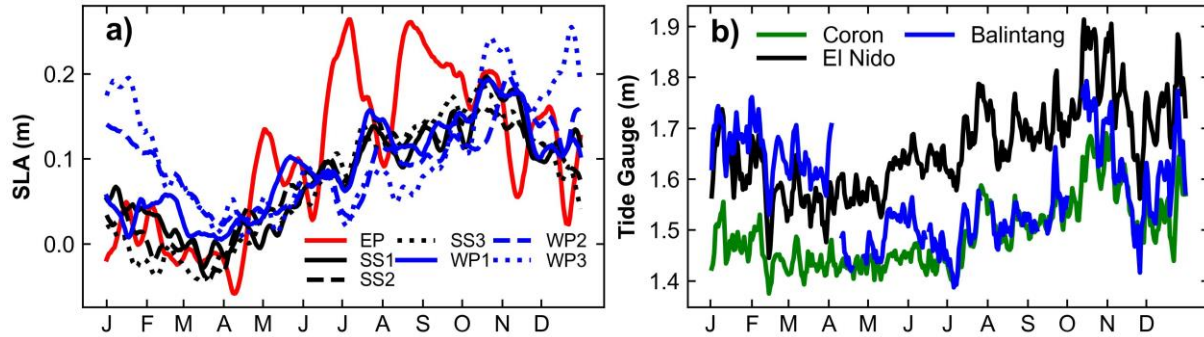


Fig. 2. (a) Time series of area-averaged daily SLA of the seven selected sites. (b) Time series of daily-averaged tide-gauge sea level records at the three Palawan stations.

131 The analysis involved examining monthly mean SLAs across the subtropical and tropical
 132 Pacific Ocean, spanning from 25°S to 25°N and from 110°E to 70°W. Signals of considerable
 133 magnitude, with absolute values > 0.2 m, were the focus of this analysis. A spatial low-pass filter
 134 achieved by an area mean of every 9×9 grids was applied to remove high-wavenumber features
 135 from the SLA maps (Fig. 3a–h). A Hovmöller diagram is plotted using the monthly mean SLA,
 136 meridionally averaged between 4.875° and 5.625°N, spanning across the Pacific Ocean from
 137 110°E to 70°W (Fig. 4a). The linear propagation speed of the SLA signal is estimated from the
 138 slope of each SLA signal (yellow dashed line in Fig. 4a). A wavelet power spectrum using
 139 Morlet wavelet is plotted using a 5-year (2015–2019) daily SLA average within the range of
 140 4.875°–5.625°N and 130°E–80°W (Fig. 4b) following the method of (Torrence & Compo,
 141 1998).

142 To quantify the characteristics of the Rossby waves, a wavenumber-frequency spectrum
 143 similar to the computation and illustration presented in Jan et al. (2021) is generated using a 20-
 144 year (2001–2020) daily SLA time series. The zonally SLA time series, spanning from 130°E to
 145 80°W, is the SLA average within the latitudinal band of 4.875° to 5.625°N (Fig. 4c and d). The
 146 dispersion relation of Rossby waves (red, yellow, and blue dashed lines in Fig. 4c and d) is
 147 computed using the equation (Cushman-Roisin, 1994),

148

$$\omega = -\beta_0 R^2 \frac{l}{1+R^2(l^2+m^2)},$$

149

150

151

152

153

154

155

156

157

158

159

where β_0 is the Rossby parameter defined as $\beta_0 = 2\Omega \cos\varphi a^{-1}$ (Ω is the angular velocity of the earth's rotation $7.2921 \times 10^{-5} \text{ rad s}^{-1}$, φ is the latitude 5°N here, and a is the earth's radius 6371 km), R is the Rossby radius of deformation, and l and m are zonal and meridional angular wavenumbers, respectively. The theoretical zonal phase speed (white lines in Fig. 4c and d) was calculated using $C_x = \omega/l$. The dispersion relation for baroclinic Rossby radius of deformation R 180, 215, and 260 km, is overlaid on the spectrum. The three radii are based on the globally computed first baroclinic Rossby radius of deformation climatology (Chelton et al., 1998) mean (± 1 standard deviation) within the range of $4.5^\circ\text{--}5.5^\circ\text{N}$ and $130^\circ\text{E--}80^\circ\text{W}$ $215.3 \pm 28.8 \text{ km}$. The wavenumber-frequency spectrum is used to examine the estimated Rossby wave speed and detect westward propagating SLA energy signals corresponding to that of the theoretical first baroclinic Rossby wave.

160

161

162

163

164

165

166

167

168

169

170

171

172

To detect the oscillation in an annual cycle, which is a characteristic of first baroclinic Rossby waves from $4^\circ\text{--}6^\circ\text{N}$ (Kessler, 1990; G. Meyers, 1979; Zang et al., 2002), the detrended SLA time series and tidal sea level records are low-pass filtered by applying a Butterworth filter with a cutoff frequency of $5.7870 \times 10^{-8} \text{ cps}$ (equivalent to 200-day period) to the time series data (Fig. 5a and b). To have a temporal and spatial view of the results obtained from Fig. 5b, the daily SLA in each grid ranging between $0^\circ\text{--}15^\circ\text{N}$ and $110^\circ\text{--}130^\circ\text{E}$ was detrended and low-pass filtered as the aforementioned procedure, and plotted as monthly mean as illustrated in Fig. 6a–i. Furthermore, a 30-day low-pass filter with a cutoff frequency of $3.8580 \times 10^{-7} \text{ cps}$ was applied to the detrended SLA time series and tidal sea level records. This processed SLA time series is used to clarify whether the observed SLA signal ($> 0.2 \text{ m}$) at 10.5°N east of the Philippines in Jan et al. (2021) was from a Rossby wave (Fig. 7a–d). The potential route of the Rossby wave penetration is also investigated. The monthly mean of low-pass-filtered SLAs within $0^\circ\text{--}15^\circ\text{N}$ and $110^\circ\text{--}180^\circ\text{E}$ are depicted in Fig. 8a–j.

173

3. Results and Discussion

174

3.1 Westward-propagating SLA signals

175

176

177

Fig. 3 shows the low-pass filtered monthly mean SLA over the tropical and subtropical Pacific Ocean. The filled blue (yellow) square and circle mark the center of the positive and negative SLA signals, respectively, in the northern (southern) hemisphere. The black (blue)

178 dashed line marks 5°N (6°S). Throughout the year 2017, noticeable basin-scale westward-
179 propagating positive and negative SLA signals were observed within the tropical Pacific band
180 ranging from 10°N to 10°S in both the northern and southern hemispheres. These SLA patterns
181 exhibit spatial and temporal characteristics consistent with Rossby waves, a finding supported by
182 analyses of satellite sea surface height observations (e.g., Chelton & Schlax, 1996; Zang et al.,
183 2002) and numerical model simulations (Fu et al., 1991; Spall & Pedlosky, 2005).

184 At 160°E (Fig. 3a), the positive SLA (crest) signifies downwelling, while at 165°W (Fig.
185 3d), the negative SLA (trough) indicates upwelling, which are the indicative pattern of Rossby
186 wave (Uz et al., 2001). These crest or trough pairs center around 5°N and 6°S , symmetrically
187 positioned concerning the equator. This alignment corresponds to the characteristic behavior of
188 the theoretical first meridional mode Rossby wave, initially proposed by Matsuno (1966) and
189 also agrees findings reported by Chelton and Schlax (1996), Delcroix et al. (1991), and Zang et
190 al. (2002), who utilized satellite-derived observations. Notably, Zang et al. (2002) observed
191 Rossby waves at 6°N and 6°S using TOPEX/Poseidon data spanning 1992–2000, differing
192 slightly from our findings of 5°N in the northern hemisphere. This difference in observed Rossby
193 wave locations may be attributed to variations in wind forcing. Kessler (1990) utilized
194 bathythermograph profiles in the northern tropical Pacific from 1970 to 1987 and found a close
195 resemblance between the amplitude pattern of wind stress curl, capable of generating Rossby
196 waves via Ekman pumping, and the depth of the 20°C isotherm (a proxy for sea surface height).
197 This similarity was particularly pronounced near 5 – 6°N , lending support to the observed location
198 of the Rossby wave noted by Zang et al. (2002) and this study. It is also worth noting that a
199 robust El Niño event occurred in 2015–2016, evidenced by the Ocean Niño Index (ONI)
200 reaching as high as 2.6 (NOAA/National Weather Service, 2023) prior to 2017. Given that
201 Rossby waves can manifest as a reflection of Kelvin waves upon reaching the eastern boundary
202 of the Pacific Ocean during El Niño events (Delcroix et al., 1994, 1991; Jacobs et al., 1994;
203 Kessler, 1990; McCreary, 1976), it is plausible that the Rossby wave observed in 2017 could
204 have originated from the 2015–2016 El Niño event.

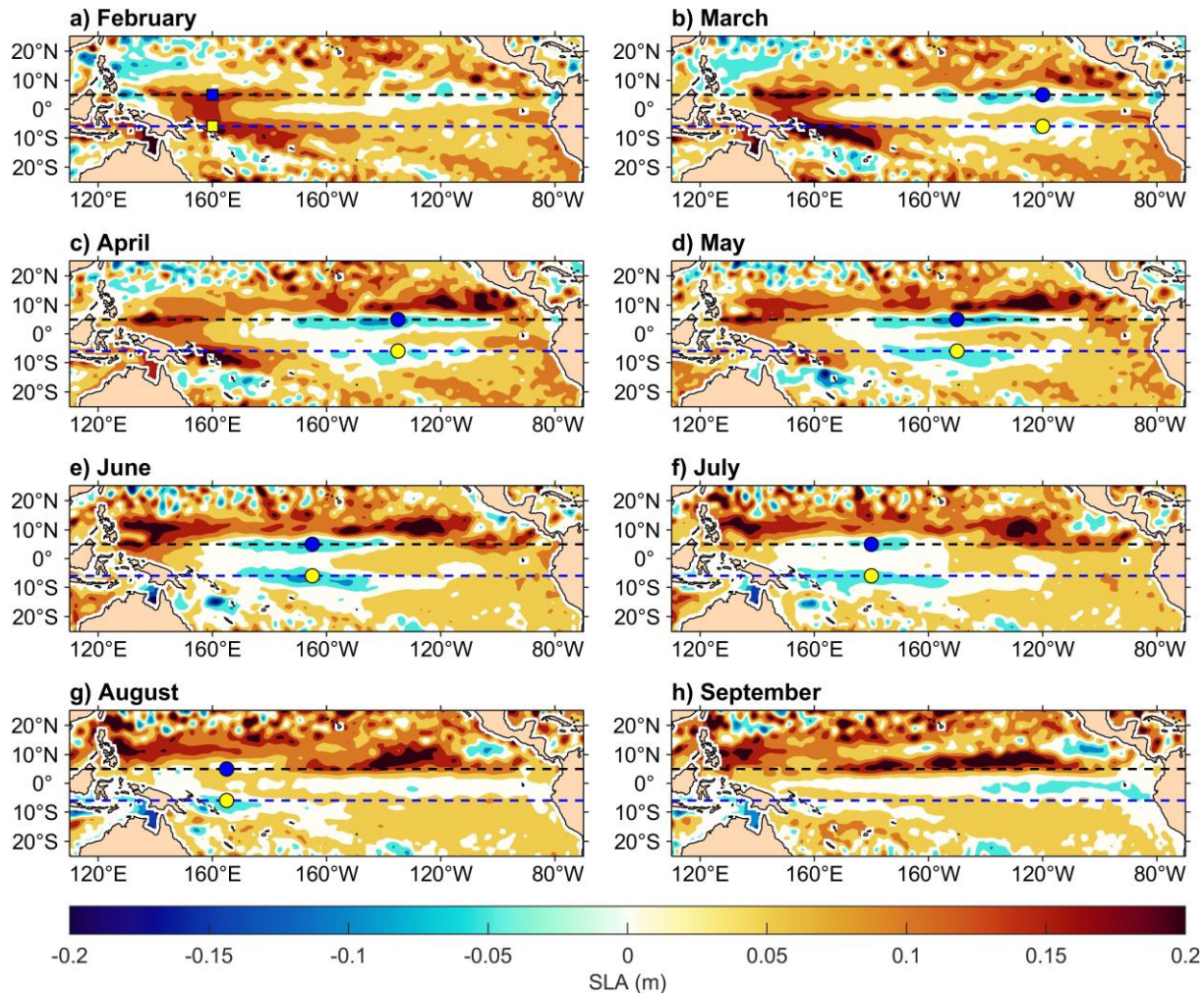


Fig. 3. Low-pass filtered satellite SLA in the subtropical and tropical Pacific Ocean. In the northern hemisphere (southern hemisphere), the filled blue (yellow) square and circle denote the centers of positive and negative SLA signals, respectively. The black dashed line represents 5°N , while the blue dashed line represents 6°S .

205 The monthly mean SLA depicted in Fig. 4a serves as the basis for calculating the phase
 206 speed of Rossby waves. These low-latitude SLA patterns observed in the northern hemisphere
 207 are anticipated to reach the east coast of the Philippines. Note that our analysis focuses on the
 208 prominent SLA signal, which manifests as a trough, indicated by the filled blue circles in Fig.
 209 3b–g. In the case of the crest, it had already translated halfway in the western boundary by April
 210 2017 (Fig. 3c), while the trough apparently propagated westward from March to July (Fig. 3b–f).
 211 The slope of the yellow dashed line in Fig. 4a corresponds to the phase speed of the Rossby
 212 wave, 0.64 m s^{-1} , at approximately 5°N . The wavelength of the Rossby wave is also estimated
 213 from Fig. 4a. The propagating distance of the crest between March and April (30 days) covered

214 15 degrees of longitude, marked by the filled yellow triangles in Fig. 4a, without considering
215 potential influences from a western boundary. In March, the Rossby wave crest and trough were
216 located at approximately 145°E and 120°W, respectively, which suggests a half wavelength of
217 ~10,545 km. Consequently, the estimated wavelength is 21,090 km. The associated period
218 estimated from Fig. 4a is approximately 12 months. Furthermore, from the wavelet power
219 spectrum of SLA in Fig. 4b illustrates SLA energy predominantly in 2017, with a period of 360
220 days.

221 The wavenumber-frequency spectrum depicted in Fig. 4c reveals the presence of energy
222 attributed to a basin-scale westward-propagating SLA with an annual period. This energy aligns
223 closely with the dispersion relation computed using baroclinic Rossby radii of 180 km
224 (illustrated by the red dashed line) and 260 km (shown as the blue dashed line) in Fig. 4c. Upon
225 magnifying the area enclosed by the black rectangle in Fig. 4d (corresponding to Fig. 4c), the
226 period associated with relatively low SLA energy (enclosed by the black oval) falls within the
227 range of 350 to 360 days. The SLA energy, close to the dispersion relation computed with a 180
228 km radius of deformation, exhibits a theoretical phase speed of approximately -0.7 m s^{-1} (the
229 negative sign implies westward propagation) and a wavenumber of approximately $-4.5 \times 10^{-8} \text{ m}^{-1}$
230 (or ~22,000 km). These values are comparable to the characteristics of the Rossby wave
231 observed in 2017. These findings are consistent with those reported by Kessler (1990) of a
232 Rossby wave near 5°N which exhibited an annual period, a zonal wavelength of ~23,000 km
233 (model estimate ~21,000 km), and a model-derived phase speed of $\sim 0.67 \text{ m s}^{-1}$.

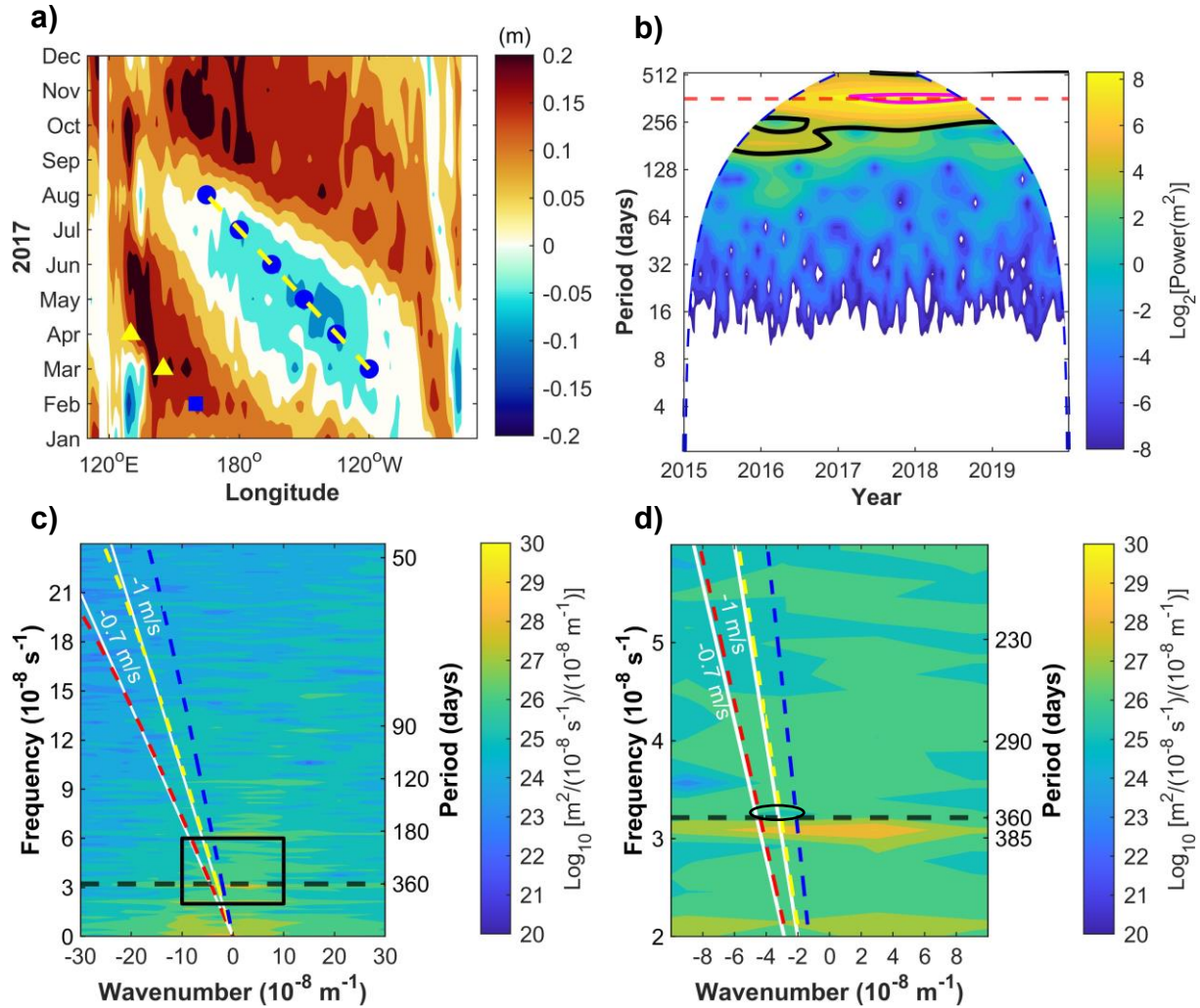


Fig. 4. (a) Hovmöller diagram illustrating satellite-derived SLA centered at 5°N . The filled blue square and circle correspond to those in Fig. 2a–g. The filled yellow triangles denote the crest centers in March and April, with the yellow dashed line indicating the phase speed of the westward-propagating negative SLA signal. (b) Wavelet power spectrum normalized by corresponding variance ($\sigma^2 = 0.0015 \text{ m}^2$). The blue dashed line indicates the cone of influence. The red dashed line denotes the 360-day period. Magenta contour is the SLA energy with approximately annual period. Black contour indicates the region with greater than 95% confidence level. (c) Wavenumber-frequency spectrum of satellite SLA. The red, yellow, and blue dashed lines are dispersion relations computed using R of 180, 215, and 260 km, respectively. The white lines show the computed theoretical phase speeds of -0.7 and -1 m s^{-1} . The horizontal black dashed line marks 360 days. (d) A close-up of the black rectangle in (c), where the black oval indicates westward-propagating (negative wavenumber) SLA energy with periods within 350 and 360 days.

234 3.2 Penetration of SLA signals through the Celebes Sea

235 Fig. 5 shows detrended and 200-day low-pass filtered satellite SLA time series off the
236 eastern Philippines (red line), in the Sulu Sea (black lines), and off the west coast of Palawan
237 (blue lines). In Fig. 5a, detrended and 200-day low-pass filtered sea level data from tide gauge
238 stations (cyan lines) are presented for comparative analysis. The low-frequency sea level
239 variations observed at WP2 (blue dashed line) and WP3 (blue dotted line) off the west coast of
240 Palawan show significant correlation with those recorded at Balintang (cyan dotted line),
241 exhibiting Pearson's correlation coefficients of 0.90 and 0.95, respectively. Moreover, WP2
242 exhibits a strong correlation with sea level variations at Coron (cyan line) and El Nido (cyan
243 dashed line), with correlation coefficients of 0.97 and 0.88, respectively. This finding suggests
244 that the satellite-derived SLA within these specific areas can effectively serve as a proxy for
245 understanding coastal sea level variations along the west coast of Palawan.

246 Further to the north, the low-frequency sea level variation at WP1 (blue line) and SS1
247 (black line) show relatively weak (correlation coefficient 0.36) and moderate (correlation
248 coefficient 0.60) correlations, respectively, with those observed at Coron (cyan line).
249 Importantly, the low-frequency sea level variation at SS1 exhibit a notably high correlation
250 (correlation coefficient 0.90) with El Nido (cyan dashed line). This finding supports that the
251 long-term variability of SLA at the major passage connecting the Sulu Sea and the SCS, the
252 Mindoro Strait, can be effectively assessed using satellite altimeter data. Therefore, the analysis
253 of detrended and low-pass filtered satellite-derived SLA proves pivotal in examining the
254 potential penetration of Rossby waves and understanding their probable pathway.

255 Fig. 5b shows that a quasi-annual sea level oscillation with period > 330 days extending
256 from February to December 2017 is clearly observed at WP2 and WP3. At WP2, the crest higher
257 than 2 cm (filled red) appears during April–May, while a trough lower than -2 cm (blue shading)
258 is noticeable during August and October. A similar pattern can be observed at WP3 but with
259 relatively higher amplitude (> 3 cm for crest and < -3 cm for trough).

260 The annual variation of SLAs at SS2 and SS3 in the Sulu Sea have similar magnitudes to
261 that at WP1 with a crest approximately 1 cm (green shading) and a trough lower than -2 cm
262 (magenta shading) around March–April and July, respectively. Note that SS1 has relatively
263 higher amplitude with a crest higher than 1 cm (brown shading) in April and a trough lower than
264 -3 cm (yellow shading) in August. The low-frequency satellite SLA at EP does not exhibit a

265 similar oscillatory pattern observed in the 2017 Rossby wave observed at $\sim 5^\circ\text{N}$. This is
 266 presumably due to the more northerly location of EP ($\sim 10^\circ\text{N}$), affecting the distinctive
 267 characteristics observed at this latitude.

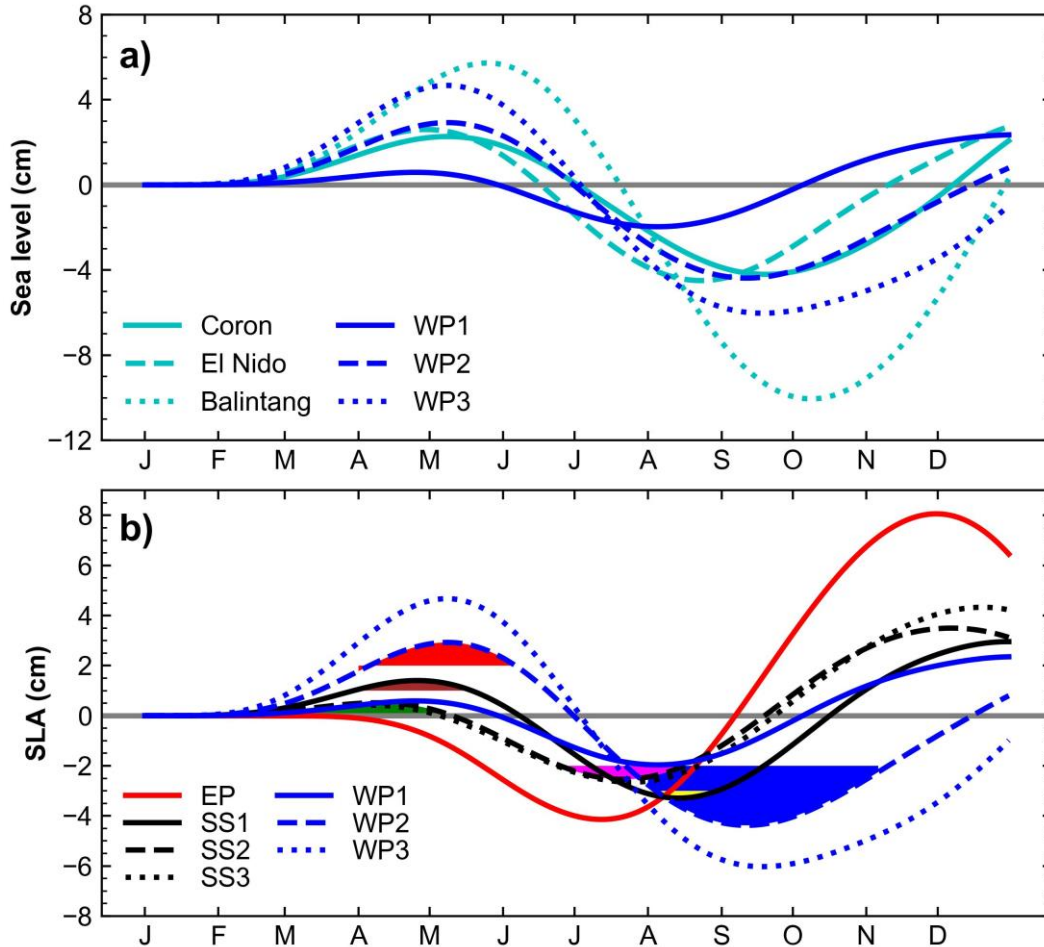


Fig. 5. (a) Time series of detrended and 200-day low-pass filtered satellite SLA and tide gauge station recorded sea levels west and north of Palawan. (b) Detrended and 200-day low-pass filtered satellite SLA across Philippines. Red and blue shadings indicate satellite SLA greater than 2 cm and lower than -2 cm, respectively, at WP2. Green and magenta shadings are satellite SLA smaller than 1 cm and lower than -2 cm, respectively, at SS2 and SS3. Brown and yellow shadings are satellite SLA greater than 1 cm and lower than -3 cm, respectively, at SS1.

268 The cross-correlation (correlation coefficient r_{SLA}) of the low-frequency satellite SLA
 269 between SS2 and EP is 0.96 at zero-lag. At WP2 and SS1, WP2 and SS2, and WP2 and WP1, the
 270 r_{SLA} is 0.77 at a 27-day lag, 0.51 at a 54-day lag, and 0.63 at a 37-day lag, respectively.
 271 Analyzing the variability of the low-pass filtered SLAs in Fig. 5b reveals that the crest (green

272 shading) and trough (magenta shading) occurrences in the northern Sulu Sea (SS2) lead those off
273 the west coast of Palawan at WP2 (red and blue shading in Fig. 5b) by 54 days.

274 This result suggests that the SLA oscillation at WP2 could be sourced from the northern
275 Sulu Sea via the Mindoro Strait. The lagged correlation between EP and SS2, however, suggests
276 that no physically plausible SLA signal penetrated from the east of the Philippines through the
277 Surigao Strait (see its location in Fig. 1a) to the Sulu Sea (SS2). The most plausible entrance of
278 the associated SLA signal is the Sibutu Passage (Fig. 1a), which connects the Celebes and Sulu
279 Seas. Results from the lagged cross-correlation analysis further suggest that, after entering Sibutu
280 Passage, the low-frequency SLA oscillation moved from SS2 to SS1 toward the Mindoro Strait
281 in the Sulu Sea. After passing through the Mindoro Strait into the central SCS, the coherent SLA
282 signal moved southward along the west coast of Palawan.

283 The pathway of the transmitted SLA signal is examined using the low-pass filtered
284 satellite SLA around the Philippine archipelago (Fig. 6a–i). In March 2017, positive SLA of
285 approximately 2 cm appeared off the west coast of Palawan, in the Sulu Sea, and the southern
286 part of the Celebes Sea (Fig. 6a). The positive SLA continuously increased to greater than 2 cm
287 in these regions and northeast of Sabah in April and May (Fig. 6b and c). As time progressed to
288 June, the SLA along the east and northern half coast of Palawan decreased to smaller than 2 cm,
289 while the southern half coast of Palawan and the southern Celebes Sea remained larger than 2 cm
290 (Fig. 6d). The SLA eventually diminished in July (Fig. 6e). The SLA pattern dramatically
291 reversed from positive to negative in August (Fig. 6f). Thereafter the SLA over these regions
292 remained negative until November (Fig. 6g–i).

293 The aforementioned results suggest that the penetration of the 2017 Rossby wave is
294 plausible, particularly for the SLA crest. It indicates that the Rossby wave transmitted into the
295 Celebes Sea at about 5°N in March (Fig. 3b). As the Rossby wave further entered the Sulu Sea
296 through the Sibutu Passage, it went along the northeast coast of Sabah and the east coast of
297 Palawan through Mindoro Strait and between Coron and El Nido. After the SLA signal passed
298 the Mindoro Strait to the SCS, SLA signal extended to the west coast of Palawan (Fig. 6d). Note
299 that a relatively higher SLA signal (> 4 cm) appeared south of Palawan, which suggests that the
300 SLA signal could also transmit through the narrow and shallow Balabac Strait. It is also noticed
301 that the SLA signal (> 2 cm) expanded to the Makassar Strait connecting the Celebes Sea and the
302 Java Sea (Fig. 6c), which is indicative of the Rossby wave transmitting toward the Indonesian

303 marginal seas as well as the Indian Ocean (du Penhoat and Cane, 1991; Spall and Pedlosky,
 304 2005). The temporal and spatial patterns of the negative SLA signal (Rossby wave trough in Fig.
 305 6f-i) are similar to those of the positive SLA signal.

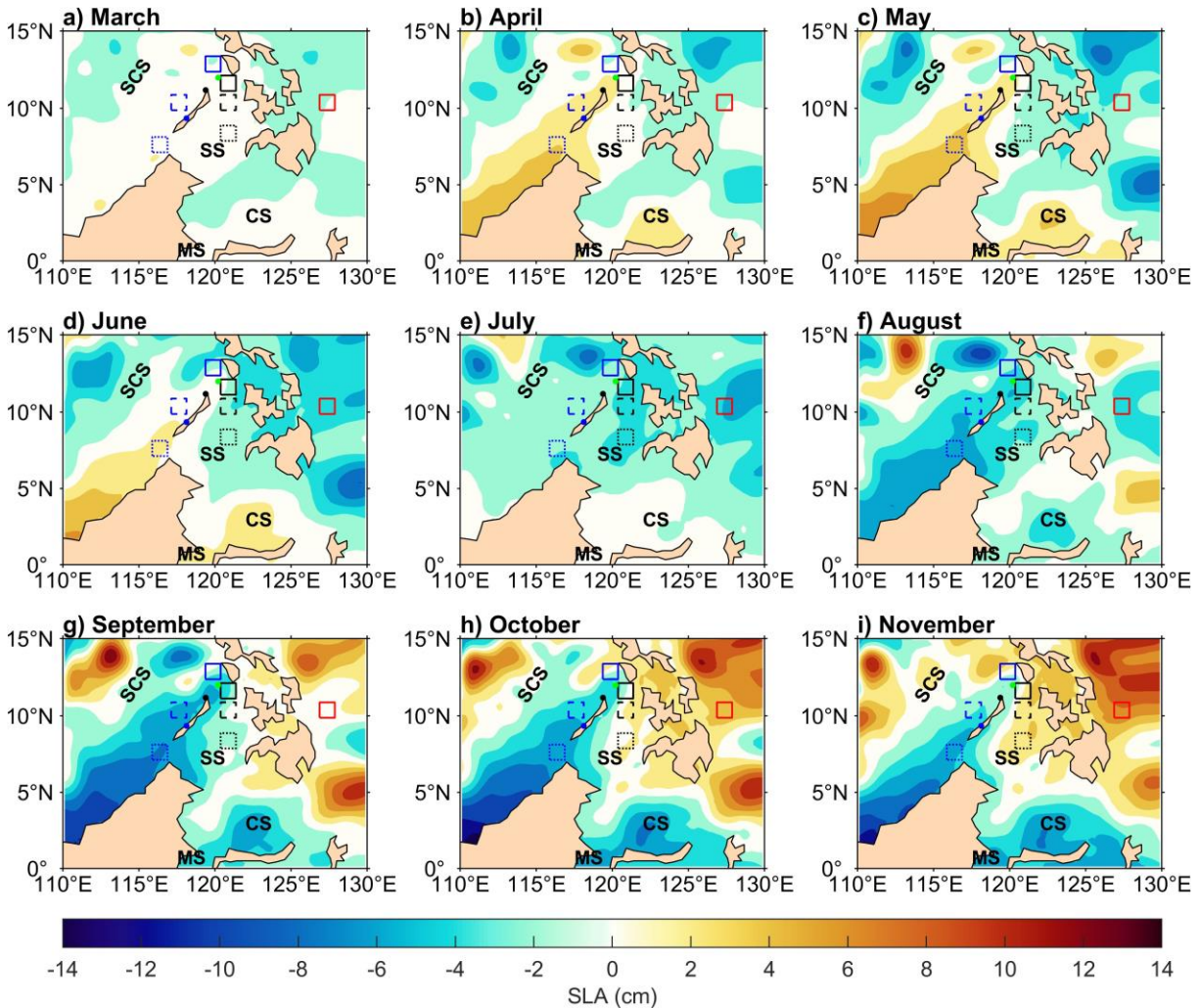


Fig. 6. Monthly mean of temporal and spatial variation in detrended and 200-day low-pass filtered satellite SLA around the Philippines. The color and line style of the rectangles correspond to those in Fig. 4b. CS means Celebes Sea, SS represents Sulu Sea, SCS represents South China Sea, and MS stands for Makassar Strait.

306 3.3 Penetration of SLA signals through Surigao Strait

307 Fig. 7 shows the detrended and 30-day low-pass filtered satellite SLA and tide gauge
 308 record time series. In the west of Palawan, this processed SLA at WP2 (blue dashed line) and
 309 WP3 (blue dotted line) are highly correlated with that at Balintang (cyan dotted line) and their
 310 correlation coefficients are 0.70 and 0.82, respectively, as the processed SLA at WP1 (blue line)

311 is highly correlated with that at El Nido (cyan dashed line) with a correlation coefficients of 0.75.
312 In the northern part of Sulu Sea, the SLA at SS1 (black line) is highly correlated with the tide
313 gauge sea level at Coron (cyan line) and El Nido (cyan dashed line), and the correlation
314 coefficients are 0.75 and 0.90, respectively. Fig. 7b–d show the SLA time series east of
315 Philippines (EP), Sulu Sea (SS1–SS3), and west of Palawan (WP1–WP3). Noticeable peaks with
316 the processed SLA greater than 10 cm appeared in the middle of July and early September 2017
317 at EP. In the Sulu Sea, SLA peaks (4–6 cm) appeared in early August and early November. West
318 of the Palawan, SLA peaks (6–10 cm) were also in early August (at WP1 only) and early
319 November (at WP1 and WP3), whereas SLA peaks at WP2 (2–6 cm) appeared in mid-August
320 and late November, which are approximately 10 days behind that of WP1. The period of
321 significant SLA oscillation (amplitude > 10 cm) at EP was during July and October (thick
322 vertical black dashed lines in Fig. 7b–d). Whereas at SS1, SS2, and WP1, the period was from
323 August to November. Additionally, significant SLA oscillation at WP2 (thin vertical black dash
324 lines in Fig. 7d), was from early August to early December, which is approximately 10 days after
325 that at SS1, SS2, and WP1.

326 The r_{SLA} of satellite SLA at SS1, SS2, and SS3 versus that of EP are 0.66 at 20-day lag,
327 0.70 at 20-day lag, and 0.73 at 15-day lag, respectively. The r_{SLA} between WP2 and WP1, SS1,
328 and SS2 is 0.60 at 10-day lag, 0.70 at 8-day lag, and 0.41 at 16-day lag, respectively. These
329 suggest that the associated SLA signal at EP leads that in the Sulu Sea, and the signal in the Sulu
330 Sea leads that off west of Palawan at approximately 20 and 10 days, respectively. The period of
331 significant SLA oscillations and lagged correlations suggest that the SLA off the eastern
332 Philippines leads that in the Sulu Sea and in turn the west of Palawan, particularly at WP2.

333 The aforementioned SLA analysis supports the hypothesis proposed by Jan et. al. (2021),
334 which suggests the penetration of Rossby waves through the Philippine archipelago to the Bohol
335 and Sulu Seas and exiting Mindoro Strait (WP1) and Balabac Strait (WP3) to the west of
336 Palawan (WP2). The Rossby waves eventually emanated from the west coast of Palawan
337 propagating westward in the central SCS. This could be the source of the fourth intraseasonal
338 velocity and satellite oscillations off Palawan and explains the weak correlation of the fourth
339 event of southwesterly monsoon strengthening during early October 2017 and the SLA rise along
340 the west coast of Palawan in November (Jan et al., 2021).

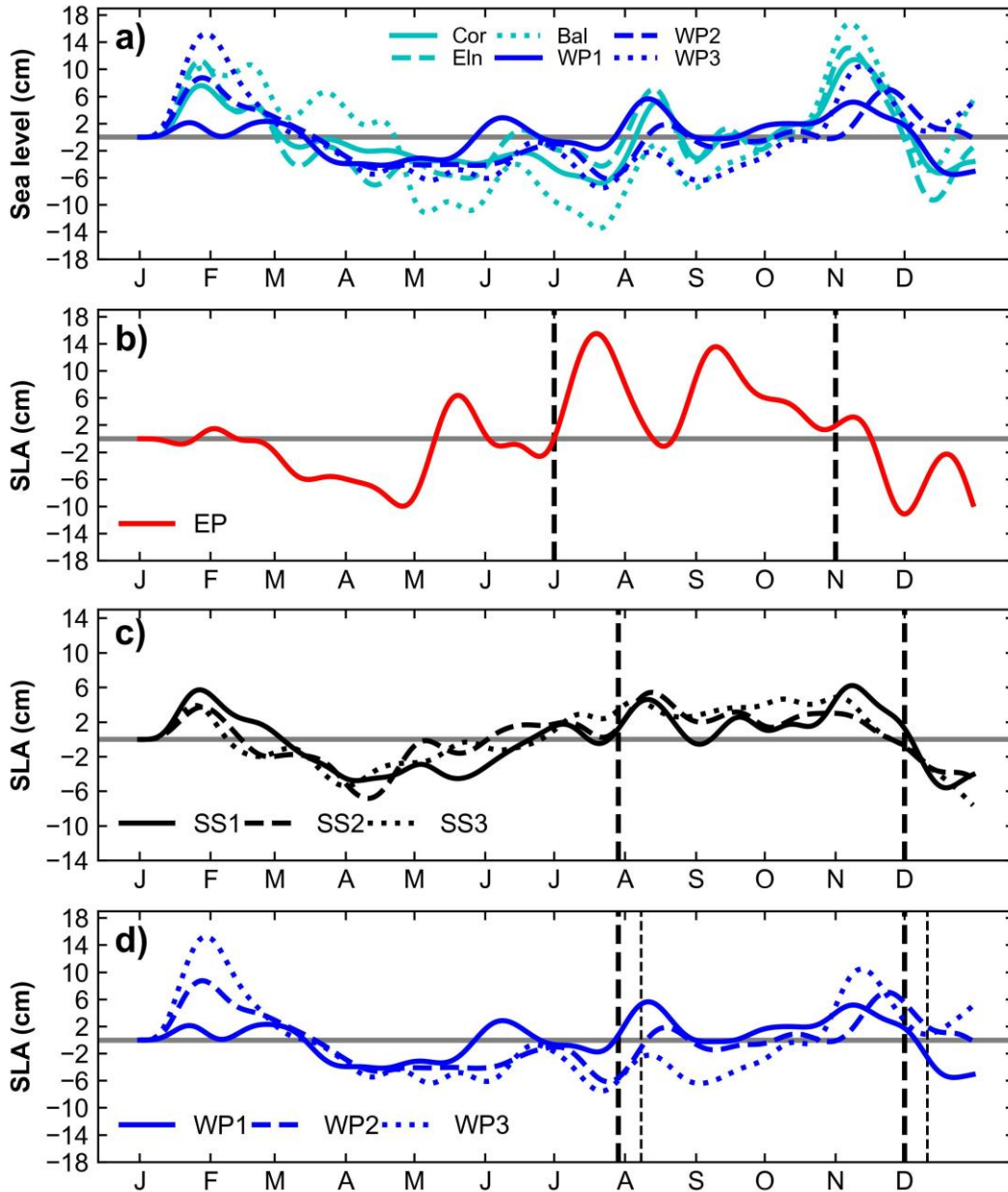


Fig. 7. (a) Time series of detrended and 30-day low-pass filtered satellite SLA alongside tide gauge station recorded sea levels west and north of Palawan. Detrended and 30-day low-pass filtered satellite SLA at (b) EP, (c) S1–S3, and (d) WP1–WP3. Thick vertical black dashed lines indicate the duration of positive SLA signal (crest). Thin vertical black dashed lines indicate the duration of positive SLA signal (crest) in WP2.

341 The peaks in the SLA variations observed east of the Philippines is verified using the
 342 temporal and spatial variations of processed SLA from the SCS to the 180°E (Fig. 8a–j). The
 343 westward-propagating positive and negative SLA signals at approximately 5°N impinged on the
 344 western boundary from April to October (Fig. 8b–h). These SLA signals observed in Fig. 3a–g

345 are verified as the first baroclinic Rossby wave, which penetrated the southern Philippine
346 archipelago (Fig. 6) and induced a quasi-annual oscillation off the west coast of Palawan (Fig. 5).
347 Between approximately 10° and 15°N , westward-propagating positive and negative SLA signals
348 impinged on the western boundary from July to December (Fig. 8e–j). These SLA signals show
349 characteristics of beta-refracted Rossby waves as those observed by Chelton and Schlax (1996)
350 and Jacobs et al. (1994). The beta-refracted Rossby waves are generated by the reflection of
351 Kelvin waves along the eastern boundary (Jacobs et al., 1994; Sirven et al., 2019). In the case we
352 analyzed, the boundary is the western coastlines of the central and north America. The wave
353 speed estimated using time-longitude plot of detrended and 30-day low-pass filtered daily SLA
354 centered at 10.5°N (i.e., 10.375° – 10.625°N average) from 130°E – 180° is approximately 0.28 m
355 s^{-1} (Figure S1), which is comparable to the first mode of baroclinic Rossby waves wave speed
356 0.2 – 0.3 m s^{-1} at about 10.5°N obtained from the theory (Chelton and Schlax, 1996) and the
357 observation (Jan et al., 2021).

358 The possible pathways of the beta-refracted Rossby wave crest transmitted across the
359 Philippine archipelago is examined using Fig. 8e–i. In July (Fig. 8e), the crest impinged on the
360 eastern Philippines, which resulted in a SLA peak greater than 10 cm east of the Philippines (Fig.
361 7b), and entered the Surigao Strait (see Fig. 1a). One month later, in August (Fig. 8f), the crest
362 progressed into the Sulu Sea via Bohol Sea and into the northern Palawan via Bohol Sea,
363 Visayan Sea, Sibuyan Sea, and Mindoro Strait, as shown by the simultaneous peaks of
364 approximately 6 cm at S1–S3 (Fig. 7c) and WP1 (Fig. 7d). Subsequently, this SLA peak moved
365 toward WP2 with approximately 2 cm height 10 days after passed WP1 (Fig. 7d). The 2 cm peak
366 at WP2 propagated westward, contributed to the second event (Fig. 1b) observed by Jan et al.
367 (2021), and consequently resulted in a decrease in SLA at WP2 (Fig. 8g and 7d) in September.
368 The trailing crest continued to propagate toward WP2 in October (Fig. 8h) and November (Fig.
369 8i). In November, the SLA crest (Fig. 8i) apparently passed WP1 (Mindoro Strait) and WP3
370 (Balabac Strait) led to a 6 cm and 8 cm peaks in early November (Fig. 7d), respectively. This
371 SLA signal eventually reached WP2 (Fig. 7d) and further propagated westward as the fourth
372 event in Fig. 1b (Jan et al., 2021). Note that the Rossby wave crest (Fig. 8e–g) at approximately
373 13°N could also pass San Bernardino Strait (S.B. Strait in Fig. 1a), Sibuyan Sea, and exit
374 Mindoro Strait and Verde Island Passage (blue star in Fig. 1a).

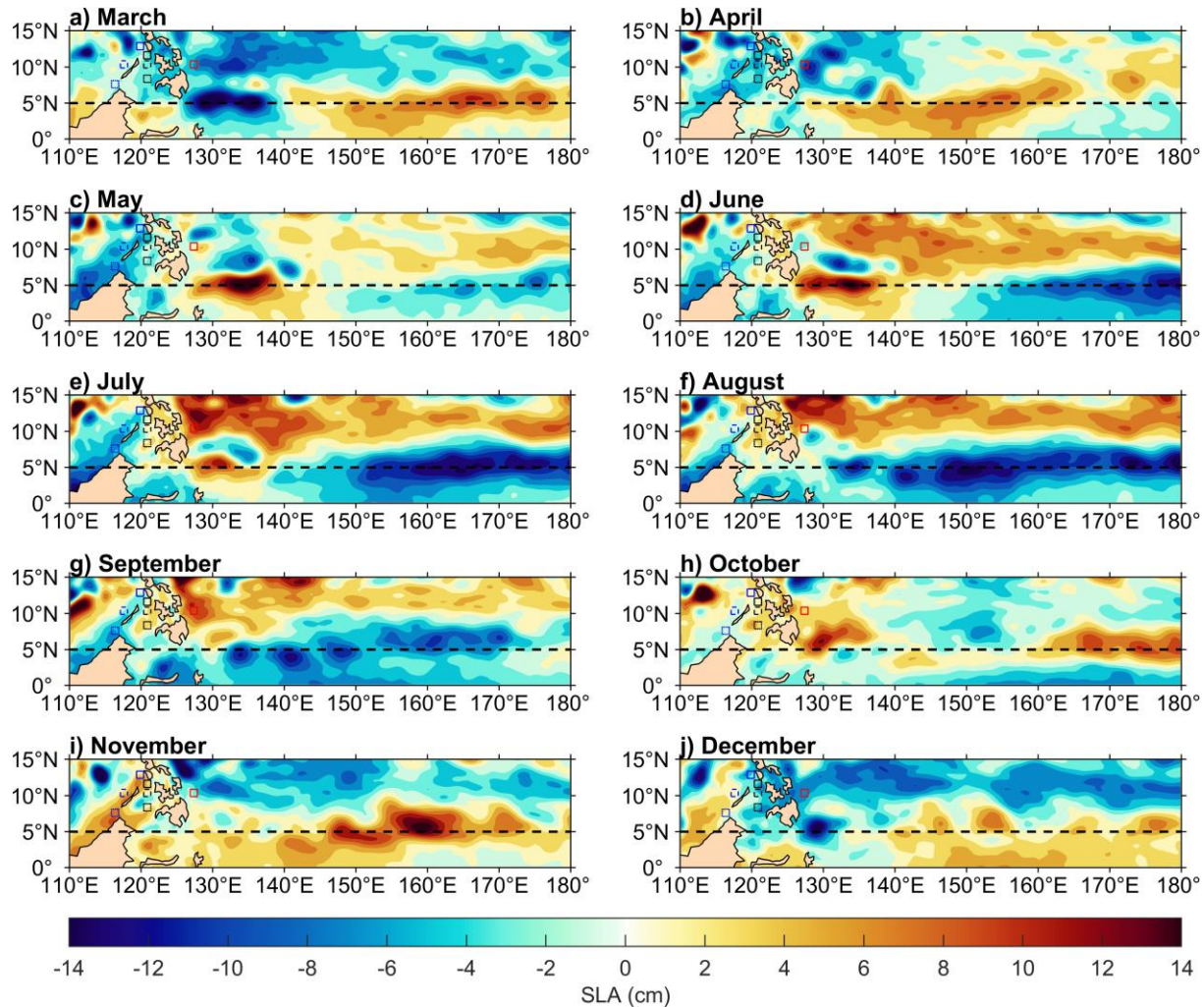


Fig. 8. Monthly temporal and spatial variations in detrended and 30-day low-pass filtered satellite SLA. The color and line style of the rectangles correspond to those presented in Fig. 7b–d.

375 4. Conclusions

376 The examination of satellite-derived SLA data, combined with sea level information
 377 gathered from fixed tide gauge stations along the Philippine coasts, delineated the westward
 378 propagation of first baroclinic Rossby waves within the tropical Pacific Ocean. This analysis
 379 revealed these waves' potential to transmit the southern Philippine archipelago and penetrate into
 380 the SCS. The estimated wave speed for the Rossby wave is approximately 0.64 m s^{-1} , exhibiting
 381 a wavelength of $\sim 21,000 \text{ km}$ and a yearly period. This wave speed is comparable to that of the
 382 Rossby waves at about 5°N , which is 0.7 m s^{-1} obtained from the theory and $\sim 0.67 \text{ m s}^{-1}$ derived
 383 from the numerical simulation (Kessler, 1990).

384 Notably, among the Rossby waves detected from satellite SLA data between 2015 and
385 2019, the 2017 Rossby wave emerged as the most prominent. This particular Rossby wave
386 translated westward along 5°N , reaching the western boundary of the North Pacific before
387 entering the Celebes Sea and proceeding into the Sulu Sea via the Sibutu Passage. The indicative
388 SLA signal of the Rossby wave hugged the northeast coast of Sabah and east coast of Palawan,
389 and passed through the Mindoro Strait and the passage between Coron and El Nido to the west of
390 Palawan. As the schematic shown in Fig. 9, the Rossby wave also passed the Makassar Strait,
391 potentially extending its influence into the Indian Ocean.

392 The temporal progression of the SLA around the Mindoro Strait also suggests that a pair
393 of cyclonic and anticyclonic eddies could be generated when the flow generated by the Rossby
394 wave passed westward through the Mindoro Strait. In addition to these findings, a β -refracted
395 Rossby wave, positioned at approximately 10.5°N , is observed with wave speed of 0.28 m s^{-1} ,
396 which is close to the theoretical speed of 0.25 m s^{-1} (Chelton & Schlax, 1996) and observed
397 speed of $0.2\text{--}0.3\text{ m s}^{-1}$ (Jan et al., 2021). The crest of this β -refracted Rossby wave impinged on
398 the east coast of the Philippines and penetrated through the archipelago through the Surigao
399 Strait. As illustrated by Fig. 8, two pathways toward west of Palawan are observed: one directed
400 southward to the Bohol Sea, Sulu Sea, and Balabac Strait and the other translated northward to
401 the Bohol Sea, Visayan Sea, Sibuyan Sea, and Mindoro Strait of Palawan island.

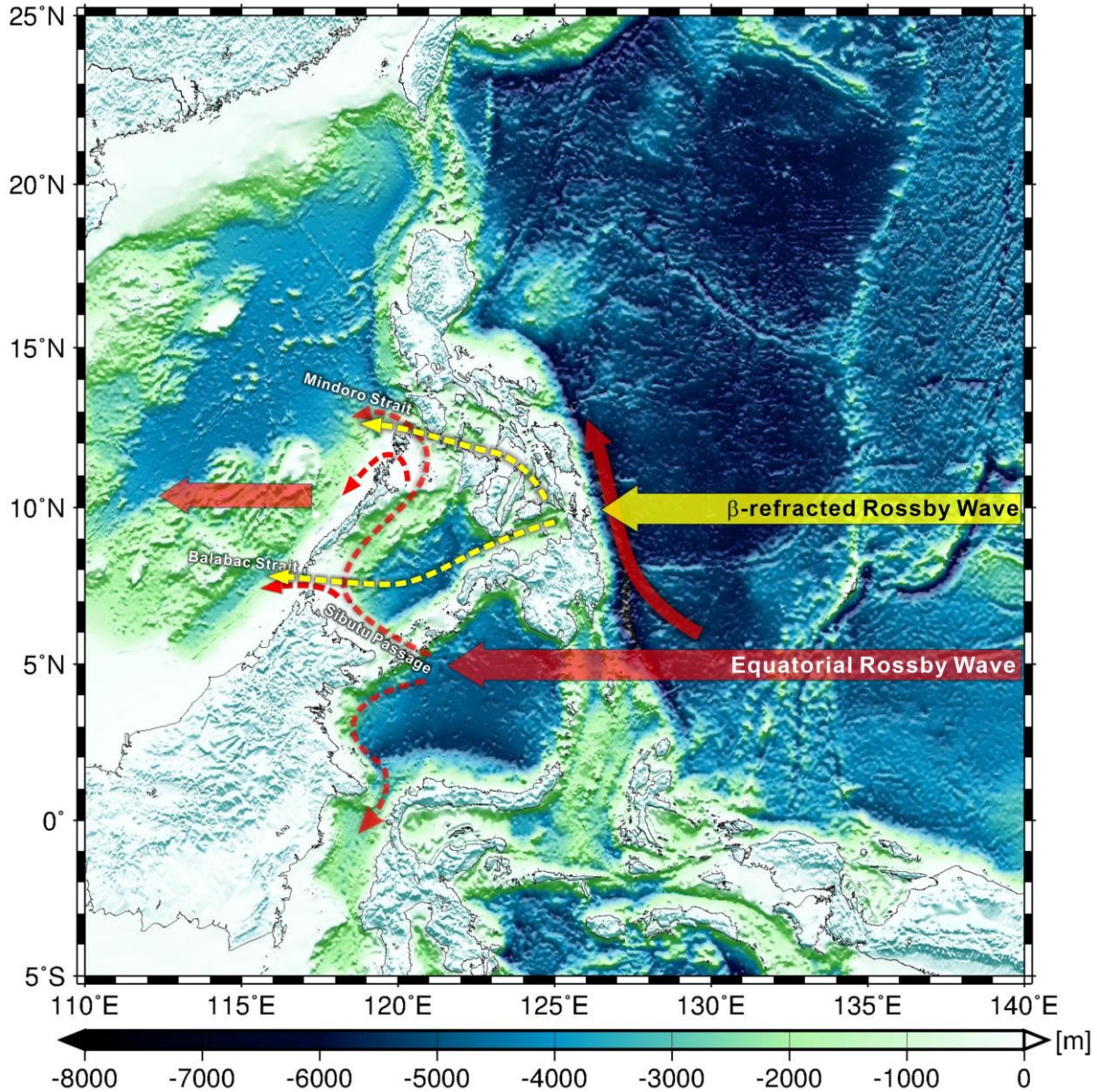


Fig. 9. A schematic diagram showing the transmission routes of both westward-propagating equatorial and β -refracted Rossby waves.

402 **Acknowledgments**

403 Yi-Chen Cheng and Yu-Yu Yeh helped plot the bathymetry chart and wavenumber-
 404 frequency spectrum, respectively. To NAMRIA Administrator Peter N. Tiangco for the hourly
 405 coastal sea level data products. This work was supported by the National Science and
 406 Technology Council (NSC) of Taiwan. SJ is sponsored under grant NSC-111-2611-M-002-020,

407 NSC-111-2119-M-002-014, and NSTC-112-2119-M-002-023. MEDM is sponsored under grant
408 NSTC-112-2119-M-002 -023. TYH is sponsored by the NSTC.

409

410 **Data Availability Statement**

411 Satellite SLA is obtained from CMEMS (accessible at <https://doi.org/10.48670/moi-00148>). Sea level records from tide gauge stations in Palawan is available at
412 <https://doi.org/10.5281/zenodo.10396727>.
413

414

415 **References**

416 Anderson, D. L. T., Bryan, K., Gill, A. E., & Pacanowski, R. C. (1979). The transient response
417 of the North Atlantic: Some model studies. *Journal of Geophysical Research*, 84(C8), 4795.

418 <https://doi.org/10.1029/JC084iC08p04795>

419 Anderson, D. L. T., & Gill, A. E. (1975). Spin-up of a stratified ocean, with applications to
420 upwelling. *Deep Sea Research and Oceanographic Abstracts*, 22(9), 583–596.

421 [https://doi.org/10.1016/0011-7471\(75\)90046-7](https://doi.org/10.1016/0011-7471(75)90046-7)

422 Cabanes, C., Huck, T., & Colin de Verdière, A. (2006). Contributions of Wind Forcing and
423 Surface Heating to Interannual Sea Level Variations in the Atlantic Ocean. *Journal of
424 Physical Oceanography*, 36(9), 1739–1750. <https://doi.org/10.1175/JPO2935.1>

425 Cabrera, O. C., Villanoy, C. L., David, L. T., & Gordon, A. L. (2011). Barrier layer control of
426 entrainment and Upwelling in the Bohol Sea, Philippines. *Oceanography*, 24(1), 130–141.

427 <https://doi.org/10.5670/oceanog.2011.10>

428 Calafat, F. M., Wahl, T., Lindsten, F., Williams, J., & Frajka-Williams, E. (2018). Coherent
429 modulation of the sea-level annual cycle in the United States by Atlantic Rossby waves.

430 *Nature Communications*, 9(1). <https://doi.org/10.1038/s41467-018-04898-y>

431 Chelton, D. B., deSzoeko, R. A., Schlax, M. G., El Naggar, K., & Siwertz, N. (1998).

432 Geographical Variability of the First Baroclinic Rossby Radius of Deformation. *Journal of
433 Physical Oceanography*, 28(3), 433–460. [https://doi.org/10.1175/1520-0485\(1998\)028<0433:GVOTFB>2.0.CO;2](https://doi.org/10.1175/1520-0485(1998)028<0433:GVOTFB>2.0.CO;2)

434

435 Chelton, D. B., & Schlax, M. G. (1996). Global Observations of Oceanic Rossby Waves.

436 *Science*, 272(5259), 234–238. <https://doi.org/10.1126/science.272.5259.234>

- 437 Cushman-Roisin, B., & Beckers, J.-M. (2011). Chapter 9 - Barotropic waves, in International
438 Geophysics, edited by B. Cushman-Roisin and J.-M. Beckers, pp. 271–315, Academic
439 Press, <https://doi.org/10.1016/B978-0-12-088759-0.00009-2>.
- 440 Delcroix, T., Picaut, J., & Eldin, G. (1991). Equatorial Kelvin and Rossby waves evidenced in
441 the Pacific Ocean through Geosat sea level and surface current anomalies. *Journal of*
442 *Geophysical Research*, *96*(S01), 3249. <https://doi.org/10.1029/90JC01758>
- 443 du Penhoat, Y., & Cane, M. A. (1991). Effect of low-latitude western boundary gaps on the
444 reflection of equatorial motions. *Journal of Geophysical Research*, *96*(S01), 3307.
445 <https://doi.org/10.1029/90jc01798>
- 446 Foreman, M.G.G. (1977). Manual for tidal heights analysis and prediction. *Pacific Marine*
447 *Science Report 77-10*, Institute of Ocean Sciences, Patricia Bay, Sidney, British Columbia.
- 448 Foreman, M.G.G. (1978). Manual for tidal currents analysis and prediction. *Pacific Marine*
449 *Science Report 78-6*, Institute of Ocean Sciences, Patricia Bay, Sidney, British Columbia.
- 450 Fu, L.-L., Vazquez, J., & Perigaud, C. (1991). Fitting Dynamic Models to the Geosat Sea Level
451 Observations in the Tropical Pacific Ocean. Part I: A Free Wave Model. *Journal of Physical*
452 *Oceanography*, *21*(6), 798–809. [https://doi.org/10.1175/1520-](https://doi.org/10.1175/1520-0485(1991)021<0798:FDMTTG>2.0.CO;2)
453 [0485\(1991\)021<0798:FDMTTG>2.0.CO;2](https://doi.org/10.1175/1520-0485(1991)021<0798:FDMTTG>2.0.CO;2)
- 454 Godin, G. (1991). The analysis of tides and currents. In: Parker, B.B. (Ed.), *Tidal*
455 *Hydrodynamics*. New York: Wiley.
- 456 Jacobs, G. A., Emery, W. J., & Born, G. H. (1993). Rossby Waves in the Pacific Ocean
457 Extracted from Geosat Altimeter Data. *Journal of Physical Oceanography*, *23*(6), 1155–
458 1175. [https://doi.org/10.1175/1520-0485\(1993\)023<1155:RWITPO>2.0.CO;2](https://doi.org/10.1175/1520-0485(1993)023<1155:RWITPO>2.0.CO;2)
- 459 Jacobs, G. A., Hurlburt, H. E., Kindle, J. C., Metzger, E. J., Mitchell, J. L., Teague, W. J., &
460 Wallcraft, A. J. (1994). Decade-scale trans-Pacific propagation and warming effects of an
461 El Niño anomaly. *Nature*, *370*(6488), 360–363. <https://doi.org/10.1038/370360a0>
- 462 Jan, S., Chang, M. H., Yang, Y. J., Sui, C. H., Cheng, Y. H., Yeh, Y. Y., & Lee, C. W. (2021).
463 Mooring observed intraseasonal oscillations in the central South China Sea during summer
464 monsoon season. *Scientific Reports*, *11*(1). <https://doi.org/10.1038/s41598-021-93219-3>
- 465 Kessler, W. S. (1990). Observations of long Rossby waves in the northern tropical Pacific.
466 *Journal of Geophysical Research*, *95*(C4), 5183–5217.
467 <https://doi.org/10.1029/JC095iC04p05183>

- 468 Matsuno, T. (1966). Quasi-Geostrophic Motions in the Equatorial Area. *Journal of the*
469 *Meteorological Society of Japan. Ser. II, 44(1), 25–43.*
470 https://doi.org/10.2151/jmsj1965.44.1_25
- 471 McCreary, J. (1976). Eastern Tropical Ocean Response to Changing Wind Systems: with
472 Application to El Niño. *Journal of Physical Oceanography, 6(5), 632–645.*
473 [https://doi.org/10.1175/1520-0485\(1976\)006<0632:ETORTC>2.0.CO;2](https://doi.org/10.1175/1520-0485(1976)006<0632:ETORTC>2.0.CO;2)
- 474 Meyers, G. (1979). Annual Variation in the Slope of the 14°C Isotherm along the Equator in the
475 Pacific Ocean. *Journal of Physical Oceanography, 9(5), 885–891.*
476 [https://doi.org/10.1175/1520-0485\(1979\)009<0885:AVITSO>2.0.CO;2](https://doi.org/10.1175/1520-0485(1979)009<0885:AVITSO>2.0.CO;2)
- 477 Meyers, S. D., Liu, M., O'Brien, J. J., Johnson, M. A., & Spiesberger, J. L. (1996). Interdecadal
478 Variability in a Numerical Model of the Northeast Pacific Ocean: 1970–89. *Journal of*
479 *Physical Oceanography, 26(12), 2635–2652.* [https://doi.org/10.1175/1520-](https://doi.org/10.1175/1520-0485(1996)026<2635:IVIANM>2.0.CO;2)
480 [0485\(1996\)026<2635:IVIANM>2.0.CO;2](https://doi.org/10.1175/1520-0485(1996)026<2635:IVIANM>2.0.CO;2)
- 481 National Oceanic and Atmospheric Administration, National Weather Service, Climate
482 Prediction Center. (2023). Cold and warm episodes by season. Retrieved from
483 https://origin.cpc.ncep.noaa.gov/products/analysis_monitoring/ensostuff/ONI_v5.php
- 484 Pawlowicz, R., Beardsley, B., & Lentz, S. (2002). Classical tidal harmonic analysis including
485 error estimates in MATLAB using T_TIDE. *Computers & Geosciences, 28(8), 929–937.*
486 [https://doi.org/10.1016/S0098-3004\(02\)00013-4](https://doi.org/10.1016/S0098-3004(02)00013-4)
- 487 Piecuch, C. G., & Ponte, R. M. (2012). Buoyancy-driven interannual sea level changes in the
488 southeast tropical Pacific. *Geophysical Research Letters, 39(5).*
489 <https://doi.org/10.1029/2012GL051130>
- 490 Qiu, B. (2003). Kuroshio Extension Variability and Forcing of the Pacific Decadal Oscillations:
491 Responses and Potential Feedback. *Journal of Physical Oceanography, 33(12), 2465–2482.*
492 <https://doi.org/10.1175/2459.1>
- 493 Sirven, J., Mignot, J., & Crépon, M. (2019). Generation of Rossby waves off the Cape Verde
494 Peninsula: The role of the coastline. *Ocean Science, 15(6), 1667–1690.*
495 <https://doi.org/10.5194/os-15-1667-2019>
- 496 Spall, M. A., & Pedlosky, J. (2005). Reflection and Transmission of Equatorial Rossby Waves*.
497 *Journal of Physical Oceanography, 35(3), 363–373.* <https://doi.org/10.1175/JPO-2691.1>

- 498 Stammer, D., Park, S., Köhl, A., Lukas, R., & Santiago-Mandujano, F. (2008). Causes for large-
499 scale hydrographic changes at the Hawaii Ocean time series station. *Journal of Physical*
500 *Oceanography*, 38(9), 1931–1948. <https://doi.org/10.1175/2008JPO3751.1>
- 501 Torrence, C., & Compo, G. P. (1998). A Practical Guide to Wavelet Analysis. *Bulletin of the*
502 *American Meteorological Society*, 79(1), 61–78. [https://doi.org/10.1175/1520-](https://doi.org/10.1175/1520-0477(1998)079<0061:APGTWA>2.0.CO;2)
503 [0477\(1998\)079<0061:APGTWA>2.0.CO;2](https://doi.org/10.1175/1520-0477(1998)079<0061:APGTWA>2.0.CO;2)
- 504 Uz, B. M., Yoder, J. A., & Osychny, V. (2001). Pumping of nutrients to ocean surface waters by
505 the action of propagating planetary waves. *Nature*, 409(6820), 597–600.
506 <https://doi.org/10.1038/35054527>
- 507 Villanoy, C. L., Cabrera, O. C., Yñiguez, A., Camoying, M., de Guzman, A., David, L. T., &
508 Lament, P. F. (2011). Monsoon-driven coastal upwelling off Zamboanga peninsula,
509 Philippines. *Oceanography*, 24(1), 156–165. <https://doi.org/10.5670/oceanog.2011.12>
- 510 White, W. B. (2000). Tropical Coupled Rossby Waves in the Pacific Ocean–Atmosphere
511 System. *Journal of Physical Oceanography*, 30(6), 1245–1264.
512 [https://doi.org/10.1175/1520-0485\(2000\)030<1245:TCRWIT>2.0.CO;2](https://doi.org/10.1175/1520-0485(2000)030<1245:TCRWIT>2.0.CO;2)
- 513 White, W. B., Chao, Y., & Tai, C.-K. (1998). Coupling of Biennial Oceanic Rossby Waves with
514 the Overlying Atmosphere in the Pacific Basin. *Journal of Physical Oceanography*, 28(6),
515 1236–1251. [https://doi.org/10.1175/1520-0485\(1998\)028<1236:COBORW>2.0.CO;2](https://doi.org/10.1175/1520-0485(1998)028<1236:COBORW>2.0.CO;2)
- 516 Zang, X., Fu, L. L., & Wunsch, C. (2002). Observed reflectivity of the western boundary of the
517 equatorial Pacific Ocean. *Journal of Geophysical Research: Oceans*, 107(10).
518 <https://doi.org/10.1029/2000jc000719>
519